Eur Biophys J (2011) 40:39–58
DOI 10.1007/s00249-010-0626-7

ORIGINAL PAPER

Membrane protein dynamics in different environments: simulation study of the outer membrane protein X in a lipid bilayer and in a micelle

Alexandra Choutko · Alice Glättli · César Fernández · Christian Hilty · Kurt Wüthrich · Wilfred F. van Gunsteren

Received: 18 June 2010 / Revised: 23 August 2010 / Accepted: 24 August 2010 / Published online: 5 October 2010

Abstract The bacterial outer membrane protein OmpX from *Escherichia coli* has been investigated by molecular dynamics simulations when embedded in a phospholipid bilayer and as a protein-micelle aggregate. The resulting simulation trajectories were analysed in terms of structural and dynamic properties of the membrane protein. In agreement with experimental observations, highest relative stability was found for the β-barrel region that is embedded in the lipophilic phase, whereas an extracellular protruding β-sheet, which is a unique structural feature of OmpX that supposedly plays an important role in cell adhesion and invasion, shows larger structure fluctuations. Additionally, we investigated water permeation into the core of the β-barrel protein, which contains a tight salt-bridge and hydrogen-bond network, so that extensive water flux is unlikely. Differences between the bilayer and the micellar system were observed in the length of the barrel and its position inside the lipid environment, and in the protein interactions with the hydrophilic part of the lipids near the lipid/water interface. Those variations suggest that micelles and other detergent environments might not offer a wholly membrane-like milieu to promote adoption of the physiological conformational state by OmpX.

Keywords Molecular dynamics · Membrane protein · Protein-water interactions · Protein-lipid interactions · Micelle bilayer comparison

A. Choutko · A. Glättli · W. F. van Gunsteren (✉)
Institute for Physical Chemistry, Swiss Federal Institute of Technology, ETH Zurich, 8093 Zurich, Switzerland
e-mail: wfvgn@igc.phys.chem.ethz.ch

C. Fernández · C. Hilty · K. Wüthrich
Institute for Molecular Biology and Biophysics, Swiss Federal Institute of Technology, ETH Zurich, 8093 Zurich, Switzerland

K. Wüthrich
Department of Molecular Biology and Skaggs Institute for Chemical Biology, The Scripps Research Institute, La Jolla, CA, USA

Introduction

Membrane proteins (MPs) constitute about 30% of all proteins in bacterial, archaean and eukaryotic organisms, where they perform a wide range of vital physiological functions (Wallin and von Heijne 1998). In apparent contrast to the wide distributions of MPs, only a smaller number of atomic-resolution structures of integral membrane proteins have been deposited in the protein data bank. Recently, however, membrane protein structural biology has made impressive progress, with important structures of α-helical and β-barrel MPs solved by X-ray crystallography and solution nuclear magnetic resonance (NMR) spectroscopy (for representative illustrations, see Cherezov et al. 2007; Gerber et al. 2008; Hanson et al. 2008; Hilf and Dutzler 2008; Hiller et al. 2008; Kadaba et al. 2008; van Horn et al. 2009). These recent advances have also led to increased interest in molecular dynamics (MD) simulations that may support the interpretation of results from experimental MP structural biology. Here we report on an MD simulation of a β-barrel MP present in the outer membrane of gram-negative bacteria.

The outer membrane serves as a protective barrier against the external environment while also controlling the flux of solutes. Proteins belonging to the outer membrane proteins (OMPs) family are composed of anti-parallel β-strands connected by short periplasmic turns and by long,

mobile loops on the extracellular side, forming a transmembrane anti-parallel β-barrel (Schulz 2002). Those proteins have a variety of functions in bacterial outer membranes such as ion transport, pathogen recognition and catalysis. With 148 amino acids, the outer membrane protein X (OmpX) represents one of the smaller members of the OMP family.

OmpX and outer membrane protein A (OmpA) from *Escherichia coli* are experimentally widely studied OMPs. The OmpX structure has been determined by X-ray crystallography (Vogt and Schultz 1999) and in a mixed protein-lipid micelle by nuclear magnetic resonance (NMR) spectroscopy (Fernández and Wider 2003; Fernández and Wüthrich 2003; Fernández et al. 2001a, b, 2002, 2004; Hilty et al. 2002, 2003, 2004). It is characterised by eight anti-parallel β-strands connected by three periplasmic turns and four extracellular loops (Fig. 1). Four of the eight β-strands protrude into the extracellular space, while in related outer membrane proteins such as OmpA, this region contains structurally disordered loops. The protruding β-sheet, also denoted as a 'waving flag' or 'fishing rod', seems to be a unique feature of OmpX and has been suggested to act as a hydrogen bonding partner to other proteins with complementary solvent-exposed β strands (Vogt and Schultz 1999). OmpA has also been studied by NMR (Arora et al. 2001; Fernández and Wider 2003; Fernández et al. 2001) and its structure was determined by X-ray crystallography (Pautsch and Schulz 2000).

Structures of membrane proteins solved by solution NMR normally originate from proteins embedded in micelles consisting of short phospholipids. These complexes have to be relatively small to allow high-resolution NMR measurements (Billeter et al. 2008; Marassi and Opella 1998). Membrane protein structures solved by X-ray crystallography require a membrane protein complexed with small detergent molecules, for example *N*,*N*-dimethyldodecylamine oxide (lauryl dimethyl amine oxide, LDAO) (Ostermeier and Michel 1997), which have only a slight resemblance to phospholipids in biological membranes. The environments needed for NMR and X-ray crystallographic measurements thus do not exactly reproduce in vivo conditions for membrane protein interactions in the physiological membrane. It is therefore of great interest that molecular dynamics (MD) simulation can provide supplementary insights into structure and dynamics in different environments using either X-ray or NMR structures of membrane proteins as the initial structure. Previous molecular dynamics studies of membrane proteins have been reported describing, among other things, the dynamic behaviour of bacterial β-barrel proteins (Domene et al. 2003; Khalid et al. 2008), the water transport in aquaporins (Hub and de Groot 2008; Hub et al. 2005), the calcium binding in the light harvesting protein bacteriorhodopsin

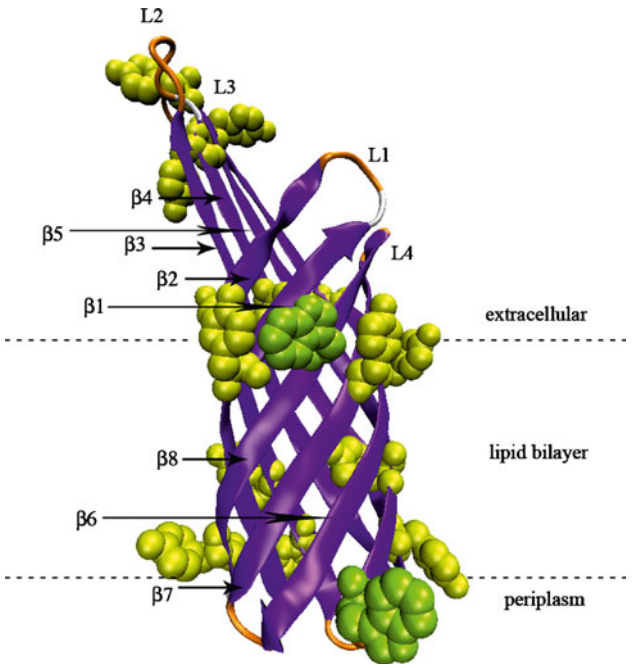

Fig. 1 Schematic diagram of the OmpX protein inserted in a lipid bilayer showing all tyrosine and tryptophan residues. The *dashed horizontal lines* represent the presumed location of the membrane. The extracellular loops are labelled (*L1–L4*). The structure shown here corresponds to the X-ray crystal structure (Vogt and Schultz 1999). The *different colors* indicate the secondary structure assignment in the crystal structure according to the definitions of secondary structure by Kabsch and Sander (1983): β-sheet *violet* [residues 2–14 (β_1), 20–32 (β_2), 37–51 (β_3), 57–72 (β_4), 77–94 (β_5), 98–116 (β_6), 121–132 (β_7), and 135–147 (β_8)], turns *orange* and random coil *white*. Tryptophans are represented in *green* and tyrosines in *yellow* space-filling models

(Wassenaar et al. 2009), the molecular mechanisms of tension-dependent channel gating (Colombo et al. 2003), and the selectivity mechanisms of ion channels (Shrivastava et al. 2002). MD simulation also offers the possibility to compare the dynamics of a membrane protein in the experimental environment, i.e. in protein/detergent co-crystals used for X-ray diffraction experiments or in protein-micelle aggregates used for solution NMR experiments, to its dynamics when embedded in a lipid bilayer, as has been done for OmpA from *Escherichia coli* (Bond and Sansom 2003).

OmpA has been widely studied experimentally and computationally (Bond and Sansom 2003; Bond et al. 2006). For OmpX we could only find a report (Böckmann and Caflisch 2005) on an equilibrium simulation of OmpX in a non-physiological aqueous solution and on non-equilibrium simulations in water/lipid mixtures, which makes comparisons of the simulated trajectories with experimental data difficult. Here we performed simulations of the OmpX protein in a lipid bilayer consisting of dimyristoylphosphatidylcholine (DMPC) molecules, and in a dihexanoylphosphatidylcholine (DHPC) micelle. As a starting structure, the NMR structure of OmpX reconstituted in

DHPC micelles was employed (Fernández et al. 2001, 2004). The resulting trajectories were analysed in terms of structural properties of the protein and regarding the level of agreement with the NMR-derived data. In particular, the flexibility of the protruding β-sheet was investigated, and an analysis of the hydrogen-bonding network in the interior of the protein and the implications for water exchange or transport properties of the protein are presented.

Overall, the specific aim of the present investigation is to gain more insights into lipid-protein and water-protein interactions in the different lipid environments. Particularly, the distribution of tyrosines (Tyr), tryptophans (Trp), arginines (Arg) and lysines (Lys) in the protein and their interactions with the lipids were investigated. This is of general interest since similar distributions of residue types (Landolt-Marticorena et al. 1993; MacCallum et al. 2008) are observed for virtually all membrane proteins as shown by statistical studies of sequence databases (Heijne 1994).

Additionally, the implications of structural and dynamic differences between OmpX embedded in a bilayer and a micelle are discussed. These considerations are of special interest as the particularities of structure determination of membrane proteins outside a phospholipid bilayer have raised discussion previously (Chou et al. 2002; Matthews et al. 2006). Detergent used to study membrane proteins may not represent the properties of the membrane bilayers very well, and it has been shown that membrane proteins embedded in micelles tend to lose their activity (Sanders and Landis 1995) and few measurements of protein activity exist for proteins in crystallographic environments. Furthermore it has been reported that certain membrane proteins do not refold to a functional state in the presence of individual lipid molecules but rather require the presence of lipid bilayers (Valiyaveetil et al. 2002).

Methods

All simulations were carried out using the GROMOS96 simulation software (Scott et al. 1999; van Gunsteren et al. 1996) and the GROMOS96 force field (version 45A3_C95) (Chandrasekhar et al. 2003; Schuler et al. 2001; van Gunsteren et al. 1996).

Molecular model

Protein and water models

Structure number 15 from the set of 20 NMR structures for OmpX obtained without hydrogen-bond restraints (PDB entry 1Q9G) (Fernández et al. 2001, 2004) was taken as the protein model. This structure corresponds to the structure with the lowest potential energy after a steepest-descent energy minimisation using the GROMOS force field and does not represent a structural outlier compared to the remaining 19 structures. The ionisable groups were set to their protonated or deprotonated state according to the standard pK_a values of amino acids and a pH of 6.8. Thus, the lysine and arginine side chains and the N-terminus were protonated, while the aspartic and glutamic acid side chains and the C-terminus were deprotonated, resulting in a net charge of $-2e$. Water molecules were modeled as rigid three-point molecules using the SPC water model (Berendsen et al. 1981).

Protein-bilayer systems

The thickness of the lipophilic phase of the outer membrane of *Escherichia coli* is estimated to be about 2.7 nm (Wimley 2002). OmpX was inserted in a dimyristoylphosphatidylcholine (DMPC) bilayer, which exhibits a lipophilic thickness of 2.6 nm at room temperature (Nagle and Tristram-Nagle 2000). To that end a bilayer of 128 DMPC lipids was pre-equilibrated in a 5 ns simulation following the simulation protocol described by Chandrasekhar et al. (2003) using the GROMOS96 force field version 45A3_C95. The phosphatidylcholine (PC) head group parameters for the partial charges in this force field were defined according to Chiu et al. (1995). The protein was then introduced in the centre of the bilayer, and 12 lipids with the largest number of van der Waals overlaps with the protein were removed from each bilayer leaflet. The total mass of the 24 removed lipids corresponds approximately to the mass of OmpX. The vertical positioning of the protein with respect to the bilayer was determined by (1) the distribution of hydrophobic and aromatic residues on the surface of the protein and (2) by the lipid-protein interactions derived from the intermolecular NOEs observed in the transverse relaxation-optimised NMR spectroscopic (TROSY) experiments of OmpX inserted in a dihexanoyl-phosphatidylcholine (DHPC) micelle (Fernández et al. 2002). In particular, the NOEs observed between the lipid headgroups and the amide protons of Met(118) and Glu(119) and the indole protons of Trp(76) and Trp(140) were used to determine the relative vertical position of the protein with respect to the bilayer-water interface.

The resulting protein-bilayer system was energy minimised to improve lipid-protein contacts using the steepest descent method while keeping the protein atoms positionally restrained. The system was then solvated in a (periodic) box using a pre-equilibrated box of SPC water resulting in a system size of over 25,000 atoms. All water molecules placed in the lipid phase in the process of solvation were subsequently removed. In simulation OmpX-DMPC-1, the protein interior does not contain any water

molecules, while in simulation OmpX-DMPC-2 the cavities of the protein are filled with water resulting in a total of 6 internal and 12 peripheral water molecules. In a further energy minimisation, water molecules were relaxed with the lipids and the protein positionally restrained. Thereafter two randomly chosen water molecules were replaced by two sodium ions to neutralise the system charge and a third energy minimisation was performed with only the protein positionally restrained.

Protein-micelle system

In the third simulation, denoted as OmpX-DHPC, the protein was inserted in a DHPC micelle, which corresponds to the system experimentally investigated by NMR (Fernández et al. 2001). As in simulation OmpX-DMPC-2, the cavities inside the protein were filled with water. The protein-micelle system was constructed by inserting the protein into a "hollow" DHPC micelle. This "hollow" micelle was obtained as follows. A large micelle consisting of 116 DMPC (not DHPC) lipids was constructed by simulating the assembly of lipids while restraining their CH_3 tails to a fixed point until the structure became spherical. From the resulting DMPC micelle, the hollow DHPC micelle was created by pruning the DMPC alkane chains to obtain DHPC chains. Thereafter the centres of geometry of the protein and of the hollow DHPC micelle were superimposed. The lipids with the largest number of van der Waals overlaps with the protein were removed, and the protein was vertically positioned using the same criteria as for the protein-bilayer system. The final micellar aggregate contains 82 DHPC lipids, which corresponds to the number of lipids estimated to be in contact with the protein from the NMR experiment (Fernández et al. 2001).

After a short energy minimisation in vacuo, the protein-lipid system was solvated in water in a (periodic) truncated-octahedron-shaped box assuring a minimum distance of 1.4 nm between the solute (OmpX + 82 DHPC lipid molecules) and the square walls of the box. The resulting system was again energy minimised to relax the surrounding water molecules followed by the replacement of two water molecules by two sodium ions and a third energy minimisation.

Simulation protocol

The MD simulations were started by taking initial velocities from Maxwellian distributions at 300 K for the bilayer systems and at 50 K for the micellar system. Solvent and solute (protein-lipid system) were independently coupled to a temperature bath with a relaxation time of 0.1 ps (Berendsen et al. 1984). The pressure was calculated using a molecular virial and held constant by weak coupling to a pressure bath with a relaxation time of 0.5 ps and using an isothermal compressibility of 4.575×10^{-4} $(\text{kJ mol}^{-1}\ \text{nm}^{-3})^{-1}$. Note that for all the equilibration simulations where the protein was positionally restrained, the simulations were performed at constant volume (NVT). Thus no pressure coupling was applied in these cases. Bond lengths and the geometry of the water molecules were constrained using the SHAKE algorithm (Ryckaert et al. 1977) with a geometric tolerance of 10^{-4}. The equations of motion were integrated using the leap-frog algorithm and a time step of 2 fs. Centre of mass motion was removed every 20 fs. The interaction between atoms in so-called charge groups (van Gunsteren et al. 1996) was calculated according to a spherical triple-range cutoff scheme: Short-range van der Waals and electrostatic interactions were evaluated at every time step by using a charge-group pair list that was generated with a short-range cutoff radius of 0.8 nm between the centres of geometry of the charge groups. Longer-range van der Waals and electrostatic interactions, between pairs at a distance longer than 0.8 nm and shorter than a long-range cutoff of 1.4 nm, were evaluated every fifth time step, at which point the pair list was also updated, and were kept unchanged between these updates. To approximate the electrostatic interactions beyond the long-range cutoff, a Poisson-Boltzmann reaction field force was used. The value for the dielectric permittivity of the continuum outside the long-range cutoff was set to 54.0 (Smith and van Gunsteren 1994), following the protocol standardly used for lipid bilayer simulations (Chandrasekhar et al. 2003).

For the two simulations of OmpX embedded in a lipid bilayer, the atoms of the protein were positionally restrained using a harmonic restraining force with a force constant of 2.5×10^4 kJ mol^{-1} nm^{-2} during the 120 ps of equilibration before adding the counter-ions. After the addition of counter-ions as described above, the system was further equilibrated for 120 ps, while the force constant of the restraining force was step-wise reduced to zero. At this point the pressure coupling was switched on and another equilibration period of 200 ps was added before saving configurations for analysis. This results in a total equilibration time of 440 ps.

For the simulation of OmpX in a micelle, the equilibration process was as follows. After addition of the counter-ions, the system was equilibrated for 60 ps during which the temperature was stepwise increased to 300 K and the restraining force decreased until the atoms of the protein were unrestrained. After this initial equilibration the pressure coupling was switched on and a further equilibration simulation of 240 ps was performed before entering the production phase. This results in a total equilibration time of 300 ps.

Analysis

The analyses were performed on the ensemble of system configurations extracted at 0.5 ps time intervals from the simulations, if not otherwise stated.

Least-squares fitting of atomic coordinates for the calculation of structural properties of the protein such as the root-mean-square deviation (rmsd) and the atomic isotropic B-factors was based on the C^{α} atoms of all residues (1–148) of OmpX. The atomic isotropic B-factors were calculated using

$$B_i = \frac{8\pi}{3}\left\langle (\mathbf{r}_i - \langle \mathbf{r}_i \rangle)^2 \right\rangle \quad (1)$$

where the brackets $\langle ... \rangle$ denote averaging.

The secondary structure assignment of OmpX for the set structures extracted every 50 ps from the simulation trajectories was done according to the DSSP rules proposed by Kabsch and Sander (1983).

Inter-proton distances derived from the NOE intensities at 300 K were compared to the corresponding average effective inter-proton distances in the simulations calculated using $\langle r^{-3} \rangle^{-1/3}$ averaging of the instantaneous inter-proton distances r. The inter-proton distances involving aliphatic hydrogen atoms were calculated by defining virtual (for CH_1 and prochiral CH_2) and pseudo (for CH_3 and non-stereospecific CH_2) atomic positions at the time of analysis (van Gunsteren et al. 1996). Pseudo-atomic distance bound corrections as defined in van Gunsteren et al. (1996) were applied using their values.

The minimum average distances between specific protein and lipid atoms were used as an approximation for the presence of NOE signals, as no exact NOE-derived distance bounds were available (Fernández et al. 2002). The minimum average distances between methyl groups or between amide or indole protons were calculated from the MD simulations as follows. The averages of specific distances were taken over the whole simulation time. However, because every lipid has two tails, the shortest average distance was chosen between one lipid tail and the protein amide or indole protons of specific residues. Analogously, for methyl groups of valines, leucines and isoleucines, the shortest average distance was taken between one of the methyl groups and the lipids.

The hydrogen bonds for the simulated and the experimental structures were calculated using a geometric criterion. A hydrogen bond is defined by a minimum donor-hydrogen-acceptor angle of 135° and a maximum hydrogen-acceptor distance of 0.25 nm.

For determining atoms distributions along the β-barrel, the positions of specific atoms were projected on a particular axis, r, within the β-barrel. The number of those specific atoms present at a specific position r along the projection axis was then calculated. The distribution g(r) corresponds to the numbers of atoms at a specific distance r and was calculated according to three methods.

In method A for DMPC the axis r is perpendicular to the bilayer. Its origin is at the centre of the bilayer. For DHPC the distribution is for spherical shells around the origin, which is the centre of the micelle.

In method B the water distribution inside the β-barrel was calculated by projecting the positions of water molecules inside the barrel on the axis along the β-barrel, passing through the centre of the cylindric β-barrel. The origin of this axis was defined as the centre of geometry of the N_H atoms of residues 6, 29, 40, 69, 80, 115, 123 and 145, which lie on a ring on one of the extremes of the β-barrel. The water molecules inside the barrel were identified as follows. The positional vector of the water molecule ($\mathbf{r}_{H_2O}$) has to fulfill the following two equations,

$$0 < (\mathbf{r}_{H_2O} - \mathbf{r}_{down}) \cdot (\mathbf{r}_{top} - \mathbf{r}_{down}) < |\mathbf{r}_{top} - \mathbf{r}_{down}|^2, \quad (2)$$

and

$$\left| \left(\mathbf{r}_{H_2O} - \frac{\mathbf{r}_{top} + \mathbf{r}_{down}}{2} \right) \times (\mathbf{r}_{top} - \mathbf{r}_{down}) \right| < \left| \left(\mathbf{r}_{side} - \frac{\mathbf{r}_{top} + \mathbf{r}_{down}}{2} \right) \times (\mathbf{r}_{top} - \mathbf{r}_{down}) \right|, \quad (3)$$

where $\mathbf{r}_{H_2O}$ is the positional vector for the oxygen water atom, $\mathbf{r}_{down}$ and $\mathbf{r}_{up}$ are the positional vectors for the periplasmic (centre of geometry of the N_H atoms of residues 6, 29, 40, 69, 80, 115, 123, 145) and the extracellular (centre of geometry of the N_H atoms of residues 13, 22, 47, 63, 87, 107, 131, 138) centres of the β-barrel respectively, and $\mathbf{r}_{side}$ corresponds to the N_H atom of residue 66, which is located at the centre of the barrel on the surface of the protein.

In method C the distribution along the β-barrel of atoms closest to the central axis of the β-barrel (as defined before) was calculated by projecting the positions of atoms less than 2 nm from the axis along the barrel that goes through the centre of the β-barrel. The origin is chosen close to the centre of the bilayer or micelle.

Results and discussion

A total of three simulations were performed. In two simulations the protein OmpX was inserted in a lipid bilayer (simulations OmpX-DMPC-1 and OmpX-DMPC-2, Fig. 2) and in one simulation we studied the micellar protein-lipid aggregate used for the NMR structure determination (simulation OmpX-DHPC). The protein in the simulation OmpX-DMPC-1 initially contains no water in the internal cavities of OmpX, while in the simulations OmpX-DMPC-2

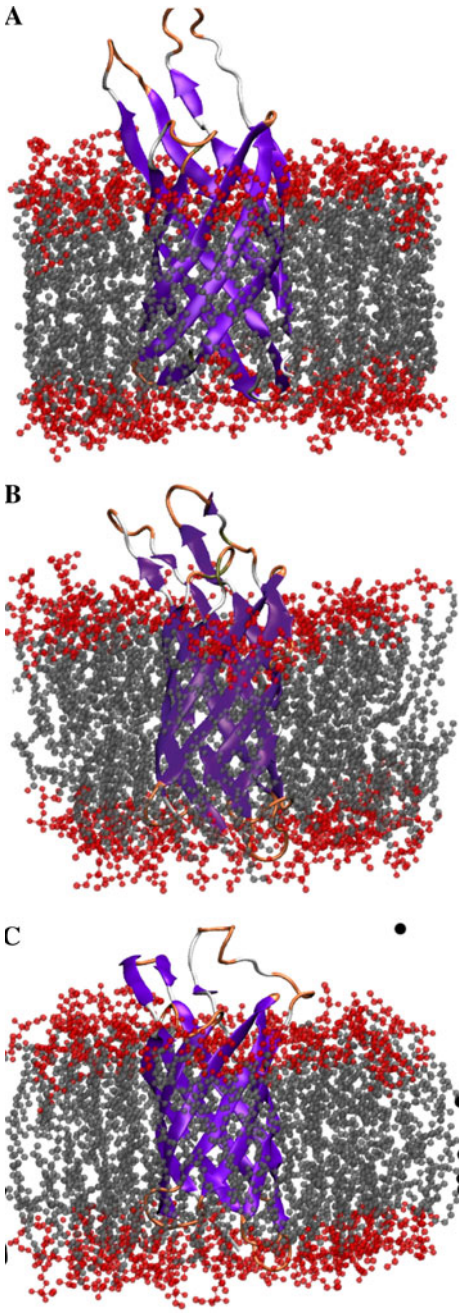

Fig. 2 OmpX protein inserted in a lipid bilayer. The structure shown here corresponds to the NMR structure 15 (Fernández et al. 2004) which was used as a starting structure. A snapshot is shown at the beginning (**a**) and at the end of the simulations OmpX-DMPC-1 (**b**) and OmpX-DMPC-2 (**c**). The *different colors* indicate the secondary structure assignment according to the definitions of secondary structure by Frishman and Argos (1995). Lipid head groups are represented in *red* and lipid side chains in *grey* space-filling models

and OmpX-DHPC these cavities are initially filled with water. An overview of the simulations is given in Table 1. In this section, the results of the analysis of structural and dynamic properties of the protein, the lipids and the water molecules are presented. Root-mean-square deviations (rmsd) of the simulated atomic trajectories relative to the initial structure and the occurrence of regular secondary structures are presented as a function of time.

The simulation trajectories are compared to the nuclear Overhauser effect (NOE) upper-bound distances derived from transverse relaxation-optimised spectroscopy (TROSY)-type NMR experiments (Fernández et al. 2004). Intramolecular hydrogen bond properties of the backbone and the side chains are presented and compared to the hydrogen bonds identified in the X-ray (Vogt and Schultz 1999) and NMR (Fernández and Wüthrich 2003) molecular models. Additionally, protein-water and protein-lipid hydrogen bonds are analysed. Finally the spatial distributions of the atoms of the protein, the water and the phospholipids across the lipid layers are analysed and differences between the micellar and bilayer systems are discussed.

General structural analysis

The time-evolution of the atom-positional rmsd values of the three simulation trajectories from the starting NMR structure are displayed in Fig. 3, and the corresponding rmsd values of the three simulation trajectories from the X-ray structure are shown in Fig. 4.

While the β-barrel and the periplasmic turns appear to be rather stable over the course of all three simulations, the extracellular loops show much larger root-mean-square fluctuations, resulting in a globally rather large rmsd of 0.2–0.3 nm for all C^{α} atoms, and about 0.4 nm for all atoms in the protein. The evolution of the rmsd values of OmpX in the simulations OmpX-DMPC-1 (Fig. 3a) and OmpX-DMPC-2 (Fig. 3b) are very similar over the first 10 ns. In OmpX-DMPC-2, the extracellular loops deviate even more from the initial NMR structure at longer simulation times. This indicates that extracellular loops, which are almost completely exposed to the solvent, constitute by far the most flexible region of the protein. The initial and final positions of OmpX inside the membrane are shown in Fig. 2. The position is stable throughout the simulations and the angle between an axis through the pore and the direction perpendicular to the membrane ranges from 3° to 15° in DMPC-1 and from 4° to 18° in DMPC-2. Experimental data (Mahalakshmi and Marassi 2008) suggest an average angle of 7°. Although there appears to be no fundamental difference between the protein embedded in a bilayer or in a micelle, it seems that at the longest simulation time the extracellular loops show less deviation from the initial positions in the NMR structure in the micellar system. The rmsd values with respect to the X-ray structure display an evolution similar to those with respect to the NMR structure. The periplasmic turns appear to deviate more from the X-ray structure than from the NMR structure.

Table 1 Simulation setups for the three simulations OmpX-DMPC-1, OmpX-DMPC-2 and OmpX-DHPC

System/simulation	OmpX-DMPC-1	OmpX-DMPC-2	OmpX-DHPC
Lipid and assembly type	DMPC, bilayer	DMPC, bilayer	DHPC, micelle
Number of lipids	104	104	82
Number of water molecules	6,518	6,559	12,682
Number of counter-ions	2 Na^+	2 Na^+	2 Na^+
Total number of atoms	25,876	25,999	42,044
Type of box	Rectangular	Rectangular	Truncated octahedron
Box size (nm^3)	5.8 × 6.3 × 9.2	5.8 × 6.3 × 9.5	9.9 × 9.9 × 9.9
Equilibration time (ns)	0.44	0.44	0.3
Simulation (production) time (ns)	15	25	25

In simulation OmpX-DMPC-1, the inside of the β-barrel is initially empty, whereas in simulations OmpX-DMPC-2 and OmpX-DHPC, the interior of the β-barrel is initially filled with water molecules. The box dimensions for the truncated octahedron are indicated as the distance between the square planes

To identify the flexible regions in the protein, the rms fluctuation (rmsf) of the backbone atoms has been calculated over all three simulation trajectories and mapped onto the final configuration of each simulation. In Fig. 5, it can be seen that for all three simulations the β-barrel, in particular the region embedded in the membrane or micelle, corresponds to the region in OmpX with the smallest atom-positional fluctuations, while the extracellular loops denote the regions with the largest mobility. In all simulations, loops number one (L1) and number two (L2) show the largest fluctuations. The periplasmic turns show, on average, atom-positional fluctuations smaller than 0.2 nm and are thus slightly more mobile than the atoms in the β-barrel.

The eight anti-parallel β strands are stable in all three simulations (Fig. 6), which is consistent with the relatively small rmsd of the β-barrel from the initial NMR structure and the observation that the barrel behaves as a rather rigid entity. There is some variation observed in the secondary structure preference of the extracellular region of OmpX. The β-strands β_3 (residues 37–51), β_4 (residues 57–72), β_5 (residues 77–94) and β_6 (residues 98–116) have been experimentally identified to be protruding into the extracellular space. In the simulation OmpX-DHPC, the extracellular part of the extended β-strands β_5 and β_6 appears to be rather unstable, with residues 90–115 adopting various bend- or turn-like conformations. In the simulation OmpX-DMPC-1, the residues 90–112 are observed to adopt a β-sheet conformation after 4 ns of simulation.

Accordingly, the rmsf (rmsf in Fig. 5, and the related atomic isotropic B-factors, shown in the right-hand panels of Fig. 6) are very large for this part of the polypeptide chain in the simulation OmpX-DMPC-2 (Fig. 6B-2). The isotropic B-factors calculated from the trajectories for the extracellular loops and the periplasmic turns have large values, while the B-factors for the C^α-atoms in the β-barrel are quite low. This corresponds qualitatively to the isotropic B-factors inferred from X-ray diffraction data.

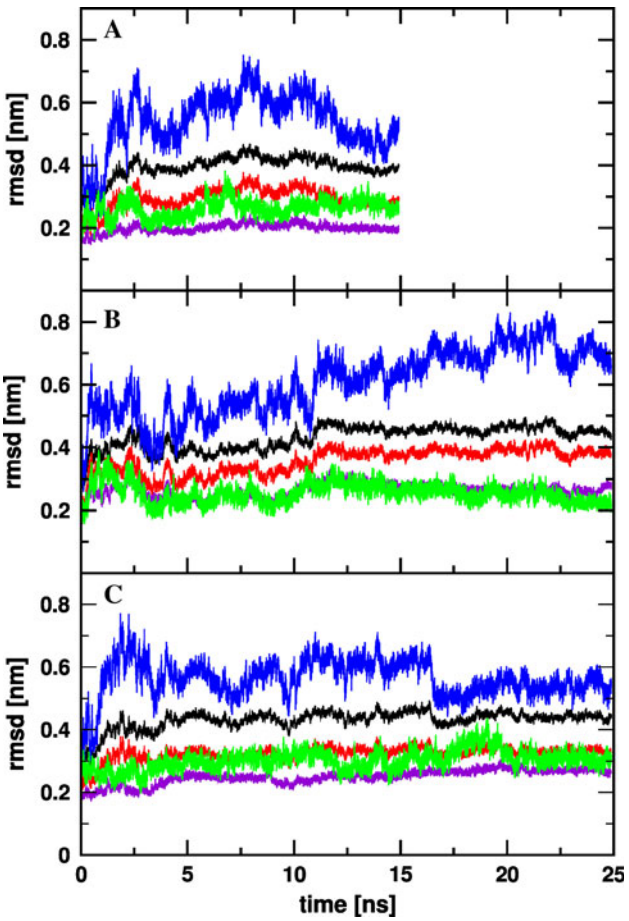

Fig. 3 Protein atom-positional root-mean-square deviations (*rmsd*) with respect to the NMR structure (Fernández et al. 2004) that was used as a starting structure for the simulations OmpX-DMPC-1 (**a**), OmpX-DMPC-2 (**b**) and OmpX-DHPC (**c**). The different lines show the rmsd calculated for all heavy atoms in the protein (*black*), for all C^α (*red*), for the β-barrel C^α atoms (*violet*), for the C^α atoms in the extracellular loops (*blue*) and for the C^α atoms in the periplasmic turns (*green*). The trajectory structures were superimposed onto the NMR reference structure by translational superposition of the protein centres of mass, followed by a least-squares rotational fit of all C^α atoms

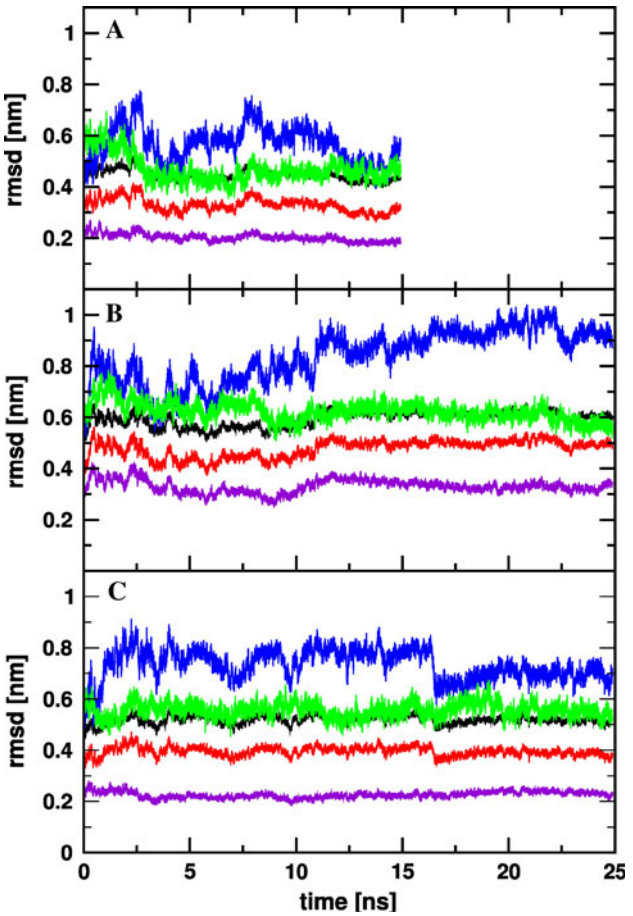

Fig. 4 Protein atom-positional root-mean-square deviations (*rmsd*) with respect to the X-ray structure (Vogt and Schultz 1999) for the simulations OmpX-DMPC-1 (**a**), OmpX-DMPC-2 (**b**) and OmpX-DHPC (**c**). The different lines show the rmsd calculated for all heavy atoms in the protein (*black*), for all C^{α} (*red*), for the β-barrel C^{α} atoms (*violet*), for the C^{α} atoms in the extracellular loops (*blue*) and for the C^{α} atoms in the periplasmic turns (*green*). The trajectory structures were superimposed onto the NMR reference structure by translational superposition of the protein centres of mass, followed by a least-squares rotational fit of all C^{α} atoms

We note that comparing crystallographically refined B-factors on the one hand with B-factors derived from the atom-positional fluctuations in a simulation or in a set of 20 NMR solution structures on the other is of limited value for a variety of reasons related to their definition, different environments, system sizes, time scales and determination techniques (Hünenberger et al. 1995; Stocker et al. 2000). An atomic X-ray crystallographic B-factor as determined in structure refinement is a quantity that differs from an atom-positional rmsf as determined from a simulation trajectory. The former quantity is an average for a specific position in the crystal over different atoms occupying that position over time or in different unit cells, whereas the latter quantity is an average for a specific atom in the crystal over its trajectory (time) positions. X-ray crystallographic B-factors are commonly restricted in size to a chosen maximum value, e.g. 1 nm^2, when varying them to optimise the agreement between calculated and measured structure factor amplitudes in structure refinement. Atom-positional rmsf from MD simulations are not restricted in size. This means that the two quantities are only of comparable size for small amplitude motion. If there is no or very little motion, the rmsf value will be smaller than the B-factor, whereas for large amplitude motion it will be much larger than the B-factor. Both cases are reflected by the data in Fig. 4.

Comparison with experimental inter-protein NOEs

OmpX is to date one of the few membrane proteins for which both crystal diffraction and NMR structural data are available. This gives us the opportunity to compare the upper-bound NOE distances inferred from experiment to the effective average inter-proton distances from the simulations. For OmpX, a total of 526 distance restraints have been derived experimentally (Fernández et al. 2004). This might seem a rather low number of NOE distance restraints for current NMR standards. However, NMR studies with large molecules or molecular assemblies require extensive deuteration to decrease transverse relaxation rates, which in turn limits the accessible ^{1}H–^{1}H-NOE distance bounds to spin systems with labile protons, i.e. to the ^{15}N–^{1}H groups (Fernández and Wider 2003; Fernández and Wüthrich 2003; Pervushin et al. 1997). The selective protonation of the Val-$\gamma^{1,2}$, Leu-$\delta^{1,2}$ and Ile-δ^{1} methyl groups enables the collection of additional NOE distance bounds from ^{15}N- and ^{13}C-resolved 3D [^{1}H, ^{1}H]-NOESY spectra. Thus, the available set of NOE distance bounds consists of distances between backbone amide proton pairs (194 distances); backbone amide and Val, Leu, and Ile methyl proton pairs (288 distances); and a few side chain–side chain proton pairs between the side chains of Val, Leu and Ile (44 distances).

For each pair of residues for which NOE information is available, the corresponding violations are shown in Fig. 7. Table 2 provides a statistical analysis of the observed violations. The overall agreement between simulation and experiment is satisfactory. Simulation OmpX-DMPC-1 fulfills 85% of the experimentally derived NOE distances. More than half of the observed 82 violations (around 60%) do not exceed 0.1 nm. Simulations OmpX-DMPC-2 and OmpX-DHPC fulfill 80% of the available NOE distances. Of the violations observed for OmpX-DMPC-2 and OmpX-DHPC about 52% are smaller than 0.1 nm. However, a number of medium- and long-range (in sequence number) NOE distances are violated in all three simulations. Most of the large violations comprise backbone–side chain proton pairs. In simulation OmpX-DMPC-1 the

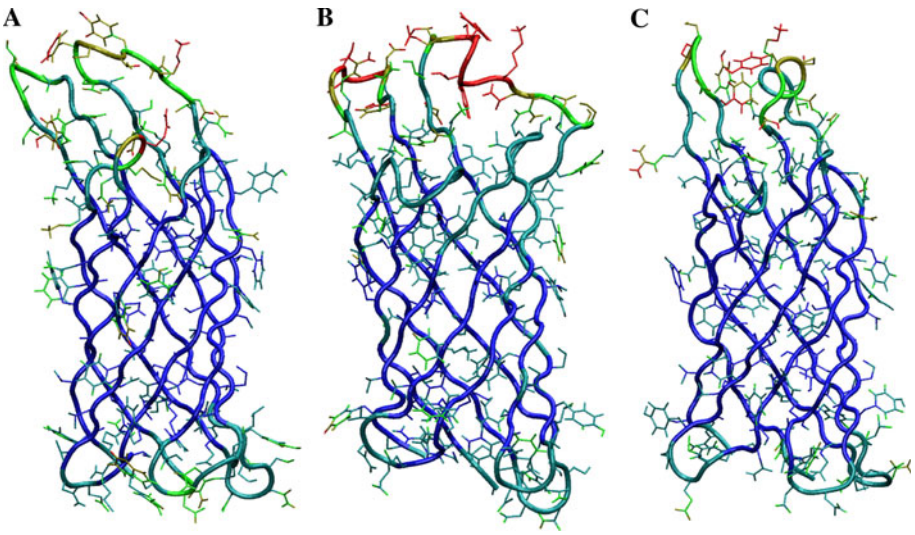

Fig. 5 Final structures of the OmpX proteins in the simulations OmpX-DMPC-1 (15 ns, **a**), OmpX-DMPC-2 (25 ns, **b**) and OmpX-DHPC (25 ns, **c**). The color shading corresponds to the root-mean-square fluctuation (*rmsf*) of the backbone atoms, *blue* ≤0.15 nm, *green* >0.15 and ≤0.35 nm, *yellow* >0.35 and ≤0.4 nm, and *red* >0.4 nm

largest six violations all involve distances between the γ^1-methyl group of Val(5) and backbone amide hydrogen atoms or side chains of residues located in the third periplasmic turn (T3) (Table 3). For simulation OmpX-DMPC-2, in addition to large violations between Val(5) and the periplasmic turn T3, large violations are also observed between the β-strands β_5 and β_6, indicating unfolding in this region of the protein. In simulation OmpX-DHPC, 6 of the 18 largest violations correspond again to NOE distance pairs between Val(5) and turn T3. The other large violations observed in simulation OmpX-DHPC correspond to distances between turn T2 and β-strand β_5 and other long-range inter-strand distances. NOE distance bounds violations observed in the single X-ray structure are quantitatively and qualitatively very similar to the violations observed for the entire trajectories (thousands of structures) of the three MD simulations. The NMR structure used as a starting structure satisfies 80% of all NOE distances, however in contrast with the X-ray structure and the three simulations almost no distance bound is violated by more than 0.3 nm.

How large must a violation of an NOE distance bound be in an MD simulation to constitute a significant disagreement between simulation and experiment? Observed violations may not be very significant since experimental NOE bounds may contain sizable uncertainties. In this regard we note a study which reported that when comparing the violation of a single MD simulation with respect to two sets of experimental NOE bounds, the MD simulation shows lower average violations for the newer, larger set of experimental bounds than with the older, smaller one (Soares et al. 2004). Between the years 1993 (old set) and 2001 (new set), the experimental data thus converged to the simulated ones, which may serve as a cautionary note when drawing conclusions about (insufficient) quality of simulated results from observed discrepancies between simulated and measured data (van Gunsteren et al. 2006).

The extracellularly protruding β-sheet shows rather large structural and spatial mobility in the simulations. It is of particular interest to monitor the long-range NOEs between neighbouring strands in this region of the protein. Due to exchange broadening in this region, only a few inter-strand NOEs could be unambiguously assigned in the NMR experiments (Fernández et al. 2004). The experimentally derived distances of these seven NOEs are listed in Table 4 together with the distance violations observed in the two sets of NMR structures and in the three simulations. A negative violation means that the distance bound is satisfied. While the NOE distances between the strands β_3 and β_4 are satisified or only weakly violated in all three simulations, one out of three NOE distance bounds between β_4 and β_5 is violated in the simulations OmpX-DMPC-1 and OmpX-DMPC-2. The violation of the NOE distance NH(88)–NH(104) in simulation OmpX-DMPC-2 clearly indicates that there is a larger distance between the strands β_5 and β_6. The protruding β-sheet region of OmpX seems to show larger fluctuations than in the sets of NMR structures. The protein-micelle simulation appears to satisfy the long-range NOE distance bounds in this area of the protein better than the simulations of the protein-bilayer system, which is to be expected since the NOE data originate from a protein-micelle aggregate.

Overall, the three simulations agree with the NOE data on the β-barrel region rather well, while inter-proton distances involving loops (in particular the loops L2 and L3) and turns, and some long-range side chain–side chain or side chain–backbone distances show larger distance violations. Additionally, when applying the pseudo-atom corrections according to Wüthrich et al. (1983), the NOE

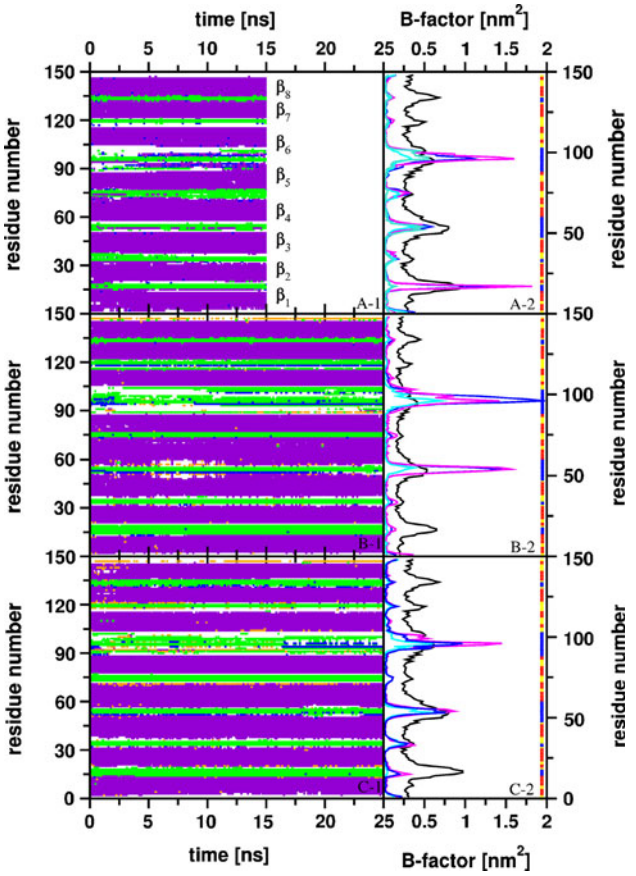

Fig. 6 *Left-hand panels* show the secondary structure of the protein as a function of time in the simulations OmpX-DMPC-1 (*A-1*), OmpX-DMPC-2 (*B-1*) and OmpX-DHPC (*C-1*). *Violet* indicates an extended strand participating in a *β*-ladder, *green* bend, *blue β*-bridge and *orange* turn, according to the definitions of secondary structure by Kabsch and Sander (1983). *Right-hand panels* show isotropic B-factors of the C^{α}-atoms as derived from the simulations OmpX-DMPC-1 (*A-2*), OmpX-DMPC-2 (*B-2*) and OmpX-DHPC (*C-2*, *blue*, *violet* and *cyan* lines) and from the X-ray diffraction data (Vogt and Schultz 1999) (*black lines*). For the simulations the B-factors were calculated over the entire trajectory (*blue*), the first half (*violet*) and the second half (*cyan*) of the trajectory. Additionally *on the far right* one can find the protein sequence color-coded as a function of the average environment of each residue: *blue* for water, *yellow* for lipids and *red* for protein

upper-bound distances are more closely satisfied in the simulations.

Lipid-protein interaction analysis and comparison with experimental data

The 28 specific distances defined by Férnandez et al. (2002) between lipids and protein amino acids are listed in Tables 5 and 6. No exact NOE distances were given in this reference but rather the presence or absence of an NOE was indicated. In order to compare the MD trajectories with these data, a distance under 0.5 nm calculated over the whole MD simulation time was assumed to produce an NOE peak. The distances calculated between the lipid carbon tails and the methyl groups of 12 valines, leucines and isoleucines (see Table 5) are in good agreement with the reported experimental data. The distances calculated between the lipid carbon tails and the amide protons of 12 amino acids satisfied more than 75% of the NOE distance bounds in the simulation OmpX-DHPC, whereas for the simulation OmpX-DMPC-2 only 33% were satisfied. This difference is readily rationalised when considering that the NMR data were measured for a protein-micelle system that corresponds closely to the OmpX-DHPC simulation. The distances calculated between the lipid *N*-methyl groups and the amide or indole protons of four amino acids (see Table 6) do not agree with those reported in Férnandez et al. (2002) for Met(118) (in bilayer and micelle simulation) and Trp(140) (in bilayer simulation). For the amino acids Glu(119) and Trp(76), the distance calculated over the entire simulation time was slightly high, however during the majority of the simulation time, this distance was below 0.5 nm. It is interesting to notice that Glu(119) did show experimental NOEs to both the lipid carbon tails and the lipid head groups in the NMR experiment [see Fig. 1 of Fernández et al. (2002)].

Intra- and inter-molecular hydrogen bonds

Figures 8 and 9 report hydrogen bonds between backbone atoms (donor amide proton and acceptor carbonyl oxygen atom) for the models built from the X-ray diffraction data and for the two sets of NMR structures (Fig. 8), and for the three ensembles of structures extracted at 0.5 ps intervals from the MD simulations (Fig. 9). The identification of hydrogen bonds is based on purely geometric criteria (see "Methods" section for details).

While the refined X-ray structure includes proper geometry for nearly all hydrogen bonds in the *β*-barrel scaffold, only a few of the implicated inter-strand hydrogen bonds in the set of 20 NMR conformers derived without explicit hydrogen-bond restraints satisfy standard criteria for this type of hydrogen bond (Fig. 8). After refinement including explicit hydrogen-bond restraints (see Fernández et al. 2004 for details), hydrogen bonds with appropriate geometry for anti-parallel *β*-sheets are seen as well in the NMR structures (Fig. 8).

In all three simulations most of the inter-strand backbone–backbone hydrogen bonds are populated between 50 and 95%, which indicates once more that the overall fold of the protein is well preserved in the simulations. Note that the simulations presented here started from the aforementioned unrefined NMR structure, where only some of the inter-strand hydrogen bonds had satisfactory geometry. Most hydrogen bonds characteristic for the *β*-barrel have

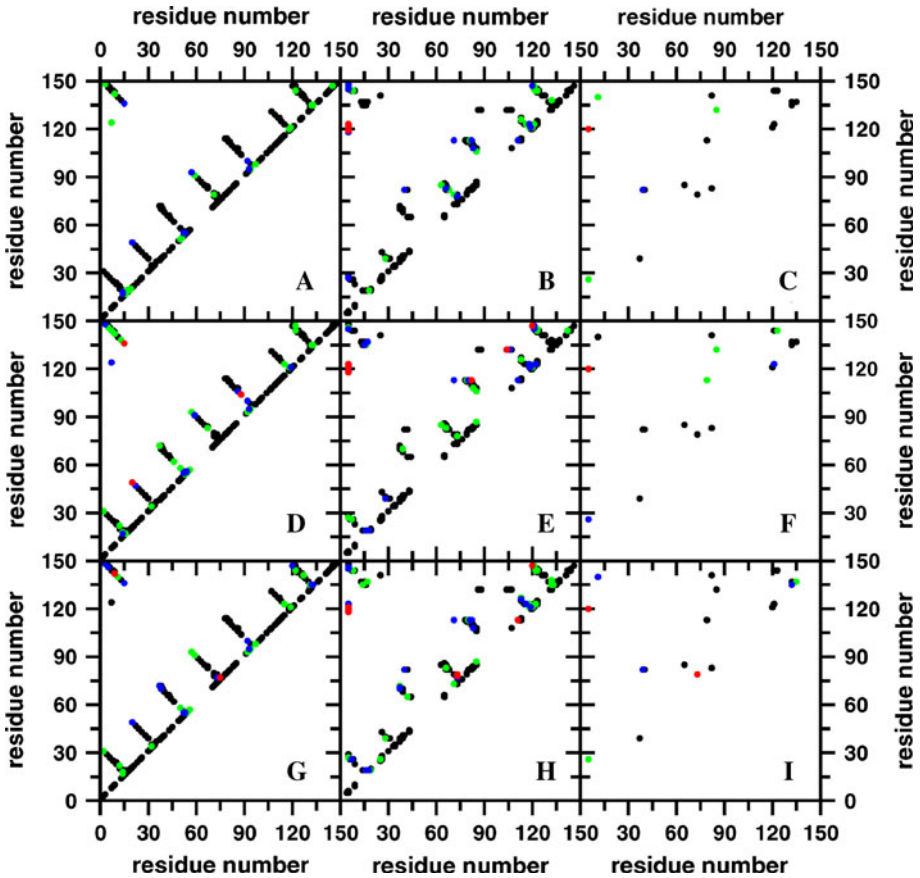

Fig. 7 Analysis of the MD trajectories with respect to the experimental NOE upper-bound distances. For each of the three simulations, the average effective violations of the NOE upper-bound distances are indicated. Simulation OmpX-DMPC-1 (**a–c**), simulation OmpX-DMPC-2 (**d–f**), simulation OmpX-DHPC (**g–i**). The 526 NOE distances inferred from the experiment are classified into three different groups. Backbone amide hydrogen pairs (194 distances) are displayed in **a**, **d** and **g**, distances between backbone amide hydrogen atoms and side chain hydrogen atoms of Val, Leu and Ile(δ^1) methyl group hydrogen atoms (288 distances) are shown in **b**, **e** and **h**, and side chain–side chain hydrogen atoms pairs (44 distances) are displayed in **c**, **f** and **i**. *Black dots* indicate hydrogen atom distances that are not violated in the simulation, *green dots* denote violations smaller than 0.1 nm, *blue dots* violations from 0.1 to 0.3 nm and *red dots* violations larger than 0.3 nm

thus been optimised in the course of the simulations. This illustrates that even though only a small number of hydrogen bonds have proper geometry, the overall β-barrel fold is correctly represented in the NMR structure employed as the starting point for the simulations and that the β-barrel fold is regularised through the unrestrained MD simulation. The β-sheet hydrogen bonds are slightly more populated in the micellar system simulation than in the bilayer simulations, which seems to be in line with experiments where NOEs were measured between OmpX and lipid molecules either in a bicelle or in a micelle (Lee et al. 2008). It would therefore be interesting to also obtain an NMR structure of OmpX in a bicelle.

In general, the inter-strand hydrogen bonds in the region of OmpX embedded in the bilayer or micelle are more populated than in the extracellular parts and the periplasmic turns of the protein. The intra-molecular hydrogen bonds in the transmembrane parts of a protein are stronger as there is no competition from the surrounding hydrocarbon tails of the lipids.

The side chains of polar and charged residues point to the interior of the β-barrel and form a network of rather stable hydrogen bonds and salt bridges (Table 7) in simulation OmpX-DMPC-1, where no water molecules are present inside the barrel during the entire simulation. This hydrogen bond network is slightly weaker in the two simulations where the barrel was initially filled with water. However, in the latter simulations a strong hydrogen bond network exists between the inner water molecules and the side chains of the protein (Table 8), which only allowed occasional exchange of a water molecule between barrel and bulk water. Consequently, there is no clear pathway between the extracellular and the periplasmic ends of the barrel, making it unlikely that a continuous water flux through the barrel will be observed. It has been suggested experimentally that OmpX is not a water pore but rather an

Table 2 Number of violations of NOE upper-bound distances for the simulations of OmpX in DMPC bilayers (OmpX-DMPC-1 and OmpX-DMPC-2) and in a micelle (OmpX-DHPC) and for the X-ray structure (Vogt and Schultz 1999) and the NMR structure (Fernández et al. 2004) used as a starting structure

Number of NOE upper bounds	Total	Range of NOE				Type of NOE		
		Intra	Sequential	Medium	Long	b–b	b–sc	sc–sc
	526	42	159	70	255	194	288	44
OmpX-DMPC-1								
Non-violated	444 (444)	42 (42)	149 (149)	54(54)	199 (199)	166 (166)	242 (257)	36 (39)
Violated by <0.1 nm	49 (49)	– (–)	10 (10)	9 (9)	30 (30)	19 (19)	26 (19)	4 (1)
Violated by 0.1–0.3 nm	27 (27)	– (–)	– (–)	7 (7)	20 (20)	9 (9)	16 (9)	2 (2)
Violated by ≥0.3 nm	6 (6)	– (–)	– (–)	– (–)	6 (6)	– (–)	4 (3)	2 (2)
OmpX-DMPC-2								
Non-violated	418 (439)	42 (42)	149 (150)	48 (51)	179 (196)	154 (154)	231 (246)	33 (39)
Violated by <0.1 nm	56 (46)	– (–)	8 (8)	9 (7)	39 (31)	25 (25)	25 (20)	6 (1)
Violated by 0.1–0.3 nm	40 (33)	– (–)	2 (1)	13 (12)	25 (20)	12 (12)	26 (19)	2 (2)
Violated by ≥0.3 nm	12 (8)	– (–)	– (–)	– (–)	12 (8)	3 (3)	6 (3)	3 (2)
OmpX-DHPC								
Non-violated	419 (439)	42 (42)	148 (151)	42 (48)	187 (198)	156 (156)	228 (246)	34 (36)
Violated by <0.1 nm	55 (41)	– (–)	10 (7)	15 (10)	30 (24)	21 (21)	33 (19)	2 (2)
Violated by 0.1–0.3 nm	38 (88)	– (–)	1 (1)	11(11)	26 (21)	15 (15)	18 (15)	5 (3)
Violated by ≥0.3 nm	14 (13)	– (–)	– (–)	2 (1)	12 (12)	2 (2)	9 (8)	3 (3)
NMR structure 15								
Non-violated	426 (457)	41 (41)	153 (154)	52 (59)	180 (203)	163 (163)	232 (256)	31 (38)
Violated by <0.1 nm	82 (58)	1 (1)	6 (5)	16 (11)	60 (41)	31 (31)	44 (25)	31 (2)
Violated by 0.1–0.3 nm	16 (11)	– (–)	– (–)	2(–)	14 (11)	– (–)	11 (7)	5 (4)
Violated by ≥0.3 nm	2 (–)	– (–)	– (–)	– (–)	2 (–)	– (–)	1 (–)	1 (–)
X-ray structure								
Non-violated	431 (454)	41 (41)	142 (144)	48 (52)	200 (217)	166 (166)	235 (254)	30 (34)
Violated by <0.1 nm	62 (46)	1 (1)	16 (14)	13 (12)	32 (19)	25 (25)	33 (17)	4 (4)
Violated by 0.1–0.3 nm	24 (18)	– (–)	1 (1)	7(4)	16 (13)	3 (3)	13 (10)	8 (5)
Violated by ≥0.3 nm	9 (8)	– (–)	– (–)	2 (2)	7 (6)	– (–)	7 (7)	2 (1)

A violation indicates that the average distance between the two hydrogen atoms, calculated as $\langle r^{-3} \rangle^{-1/3}$, is larger in the MD simulation than the one derived from the NMR experiment, r_{exp} (for details see "Methods" section). The values *in parentheses* correspond to the number of violations when applying the more generous pseudo-atom corrections established by Wüthrich et al. (1983). The NOEs are classified according to two different criteria: (1) the distance in residue sequence number: intra-residual (n:n), sequential (n:$n \pm 1$), medium-range (n:$n \pm m$, with $m = 2, 3, 4$), and long-range (n:$n \pm m$, with $m > 4$); (2) the type of hydrogen pairs: backbone–backbone pairs (b–b), backbone–side chain pairs (b–sc), side chain–side chain pairs (sc–sc)

iron pore (Lin et al. 2008), but the simulations presented here do not show any features supporting this suggestion.

The protein-water hydrogen-bond network inside the barrel shows slight differences between the membrane (DMPC-2) and the micelle (DHPC) simulations (Table 8). This can easily be induced by slight changes in the barrel structure due to the different lipid environments.

Charged or aromatic amino acids make hydrogens bonds with the lipid head groups, as can be seen in Table 9. The lipid head groups make hydrogen bonds with 12 out of 14 tyrosines and one out of two tryptophans, which are all located at the lipid/water interface. It has been suggested that amphipathic aromatic amino acids position the protein in its correct orientation within the membrane (MacCallum et al. 2008; Schulz 1993) by interaction with the lipid head groups (de Planque et al. 2003; Sun et al. 2008; Yau et al. 1998). Two aromatic residue "belts" on each side of the β-barrel can be observed in Fig. 1. The width of the lipid phase in the natural membrane and in the micelle or bilayer is therefore crucial for the proper positioning of OmpX. Indeed it has been shown that OmpX migrates to the outer membrane of *E. coli* because the outer membrane is slightly thinner than the inner membrane (Kleinschmidt and Tamm 1996). The lipid head groups make hydrogen bonds with only 4 out of the 12 arginine and lysine residues, mainly because most of these are located in the extracellular β-sheet. Those two residue types are thought

Table 3 Average NOE distance bound violations $\langle r^{-3} \rangle^{-1/3} - r_{exp}$ for all hydrogen atom pairs for which NOE distance bounds were violated more than 0.3 nm in any of the three simulations (structures of each MD simulation taken at an interval of 0.5 ps)

OmpX-DMPC-1		OmpX-DMPC-2		OmpX-DHPC	
Hydrogen atom pair	Violation (nm)	Hydrogen atom pair	Violation (nm)	Hydrogen atom pair	Violation (nm)
C_γ1(Val5)–NH(Leu123)	0.319	NH(Lys20)–NH(Ser49)	0.301	NH(Asp75)–NH(Ala77)	0.316
C_γ1(Val5)–NH(Val121)	0.411	C_γ1(Val5)–NH(Met118)	0.302	NH(Ala111)–C_δ2(Leu113)	0.337
C_γ1(Val5)–NH(Glu119)	0.440	H_δ2(Asn120)–NH(Arg147)	0.306	NH(Tyr9)–NH(Ala142)	0.360
C_γ1(Val5)–NH(Asn120)	0.444	NH(Val82)–C_δ1(Leu113)	0.320	C_δ1(Ile73)–NH(Ile79)	0.367
C_γ1(Val5)–NH(Asn120)	0.683	C_γ1(Val5)–NH(Val121)	0.322	NH(Ile73)–C_δ1(Ile79)	0.368
C_γ1(Val5)–H_δ1(Asn120)	0.737	NH(Gln15)–NH(Asp136)	0.323	C_γ1(Val5)–NH(Met118)	0.446
C_γ1(Val5)–H_δ2(Leu26)	0.300	C_γ1(Val5)–H_δ2(Asn120)	0.440	C_γ1(Val5)–NH(Val121)	0.471
		C_γ1(Val5)–NH(Leu123)	0.459	C_γ1(Val5)–NH(Asn120)	0.528
		NH(Asp104)–C_δ1(Ile132)	0.474	C_δ1(Ile73)–NH(Ser78)	0.559
		C_γ1(Val5)–H_δ2(Asn120)	0.538	H_δ2(Asn120)–NH(Arg147)	0.560
		NH(Gly88)–NH(Asp104)	0.650	C_δ1(Ile73)–C_δ1(Ile79)	0.680
				C_δ1(Val5)–NH(Glu119)	0.702
				C_δ1(Val5)–H_δ2(Asn120)	0.887
				C_δ1(Val5)–H_δ2(Asn120)	0.898

The NOEs are classified according to the type of hydrogen pairs: backbone (NH) or side chain (sc). A violation indicates that the average distance between the two hydrogen atoms, calculated as $\langle r^{-3} \rangle^{-1/3}$, is larger in the MD simulation than the distance bound derived from the NMR data, r_{exp}

Table 4 Long-range NOE upper-bound distances within the extended, protruding β-sheet at the extracellular end of the strands β_3, β_4, β_5 and β_6

NH–NH	Experimental NOE upper-bound distance (nm)	Distance bound violations				
		$\langle v \rangle_{NMR\text{-}1}$ (nm)	$\langle v \rangle_{NMR\text{-}2}$ (nm)	$\langle v \rangle_{OmpX\text{-}DMPC\text{-}1}$ (nm)	$\langle v \rangle_{OmpX\text{-}DMPC\text{-}2}$ (nm)	$\langle v \rangle_{OmpX\text{-}DHPC}$ (nm)
50–58	0.368	0.005	0.015	−0.020	0.071	0.023
52–56	0.614	−0.220	−0.225	−0.183	−0.163	−0.139
57–93	0.377	0.020	0.014	0.243	0.099	0.009
59–91	0.359	0.031	0.023	0.049	0.269	0.019
61–89	0.488	−0.063	−0.033	−0.147	−0.046	−0.217
88–104	0.425	0.007	0.015	−0.060	0.650	−0.076
92–100	0.387	0.005	0.002	0.200	0.261	0.117

NOEs identified in the NMR TROSY experiment (Fernández et al. 2004) and the average effective violations of the associated upper-bound distances calculated from the two sets of NMR model structures, without and with hydrogen-bond restraints ($\langle v \rangle_{NMR\text{-}1}$ and $\langle v \rangle_{NMR\text{-}2}$), and from the structures in the MD simulations OmpX-DMPC-1 ($\langle v \rangle_{OmpX\text{-}DMPC\text{-}1}$), OmpX-DMPC-2 ($\langle v \rangle_{OmpX\text{-}DMPC\text{-}2}$), and OmpX-DHPC ($\langle v \rangle_{OmpX\text{-}DHPC}$) are shown. The average effective distance violation is calculated as $\langle r^{-3} \rangle^{-1/3} - r_{exp}$ for the two sets of 20 NMR structures and for the structures of each MD simulation taken at an interval of 0.5 ps

to "snorkel" to the membrane surface, where they bury their aliphatic parts inside the lipophilic membrane while positioning their charged groups in the polar interface (Deol et al. 2004; Heijne 1994; Landolt-Marticorena et al. 1993; Strandberg and Killian 2003). The micellar system seems to have more hydrogen bonds of lysine and arginine with lipid head groups than the bilayer system. This might indicate that the micelle is thicker than the bilayer, enabling residues located on the extracellular β-sheet to interact with the lipids.

Atom distributions inside the membrane and the micelle

Figure 10 shows the distribution of the atoms of the protein, the lipids and the water molecules in the bilayer and in the micelle. The integral under each curve represents the total number of atoms. The atom number profile of the bilayer seems rather different from that of the micelle for geometric reasons. The atom number profile of the bilayer is as expected, with the lipophilic side chains in the centre of the membrane and the head groups in the outer part of

Table 5 Minimum average distances calculated as $\langle r \rangle$ from MD simulations (OmpX-DHPC and OmpX-DMPC-2) between methyl groups of all valines, isoleucines, leucines or amide protons of selected amino acids and lipid tail carbons

Methyl groups	OmpX-DHPC (nm)	OmpX-DMPC-2 (nm)	Experimental NOE	Amide protons	OmpX-DHPC (nm)	OmpX-DMPC-2 (nm)	Experimental NOE
Val5	0.38	0.38	Yes	Thr4	0.74	0.79	Yes
Leu26	0.38	0.38	Yes	Val5	0.60	0.65	No
Leu37	0.37	0.38	Yes	Thr6	0.50	0.51	Yes
Val39	0.38	0.38	Yes	Gly7	0.43	0.47	Yes
Ile79	0.38	0.40	Yes	Gly8	0.31	0.57	Yes
Val83	0.38	0.37	Yes	Tyr9	0.35	0.70	Yes
Leu123	0.38	0.38	Yes	Ala10	0.54	0.86	Yes
Val144	0.37	0.40	Yes	Gln11	0.47	0.82	Yes
Val135	0.86	1.18	No	Ala13	0.39	0.69	No
Val137	0.76	0.82	No	Met118	0.54	0.77	Yes
Ile40	0.78	0.67	No	Glu119	0.45	0.69	Yes
Val82	0.69	0.57	No	Asp124	0.64	0.76	Yes

The shortest distance between all lipid tail carbons and selected amino acid atoms was selected to approximate the presence of an NOE signal (see "Methods" section for details). Distances under 0.5 nm are considered to give an NOE signal. Additionally the presence (Yes) or absence (No) of an experimental NOE (Fernández et al. 2004) is indicated

Table 6 Minimum average distances calculated as $\langle r \rangle$ from MD simulations (OmpX-DHPC and OmpX-DMPC-2) between amide or indole protons of selected amino acids and lipid *N*-methyl groups

Amide or indole protons	OmpX-DHPC (nm)	OmpX-DMPC-2 (nm)	Experimental micelle (Fernández et al. 2002) NOE	Experimental bicelle (Lee et al. 2008) NOE
Met118(NH)	0.86	0.83	Yes	Yes
Glu119(NH)	0.56	0.54	Yes	Yes
Trp76(N_εH)	0.55	0.56	Yes	NA
Trp140(N_εH)	0.53	1.05	Yes	NA
Met21(NH)	0.54	0.24	No	Yes
Gly22(NH)	0.86	0.13	No	Yes
Asp75(NH)	0.55	0.55	No	Yes
Asp136(NH)	0.84	0.82	No	Yes

The shortest distance between all lipid *N*-methyl carbons and selected amino acid atoms was selected to approximate the presence of NOE signals (see "Methods" section for details). Distances under 0.5 nm are considered to give an NOE signal. Additionally the presence (Yes) or absence (No) of an experimental NOE (Fernández et al. 2004) is indicated. *NA* Not available

the membrane. For the micelle, a broader distribution of lipid atoms is present, which reflects the lack of a symmetry plane in the micelle. The protein seems to be slightly more embedded in the lipophilic part of the micelle than in the case of the bilayer. Water permeates the membrane and the micelle at the level of the head groups, which is to be expected. No water is present inside the lipophilic part of the membrane or the micelle. The little bumps in the water curve visible in Fig. 10c are due to water molecules inside the barrel, as can be verified in Fig. 11. The water present in the β-barrel seems to cluster in three to five cages distributed along the pore (Fig. 11). The strong intra-protein hydrogen bond network creates separate water spaces, as can be seen in Fig. 12. Little water exchange with the exterior is observed in the OmpX-DHPC simulation (indicated by the presence of water peaks around the edges of the OmpX-DMPC-2 but not the OmpX-DHPC β-barrel in Fig. 11). Notably, in OmpX-DMPC-1, no water molecules penetrate into the barrel during the time of the simulation.

Figure 13 shows the distribution of atoms within 2 nm of the axis of the β-barrel. The protein is slightly longer inside the micelle (7.6 nm) than inside the bilayer (7 nm). The head group distribution is broader in the micelle than in the bilayer. The micelle (6.9 nm) is thicker than the bilayer (6 nm). The lysine, arginine, tryptophan and tyrosine side chains have a broader distribution in the micelle than in the bilayer because those amino acid residues prefer

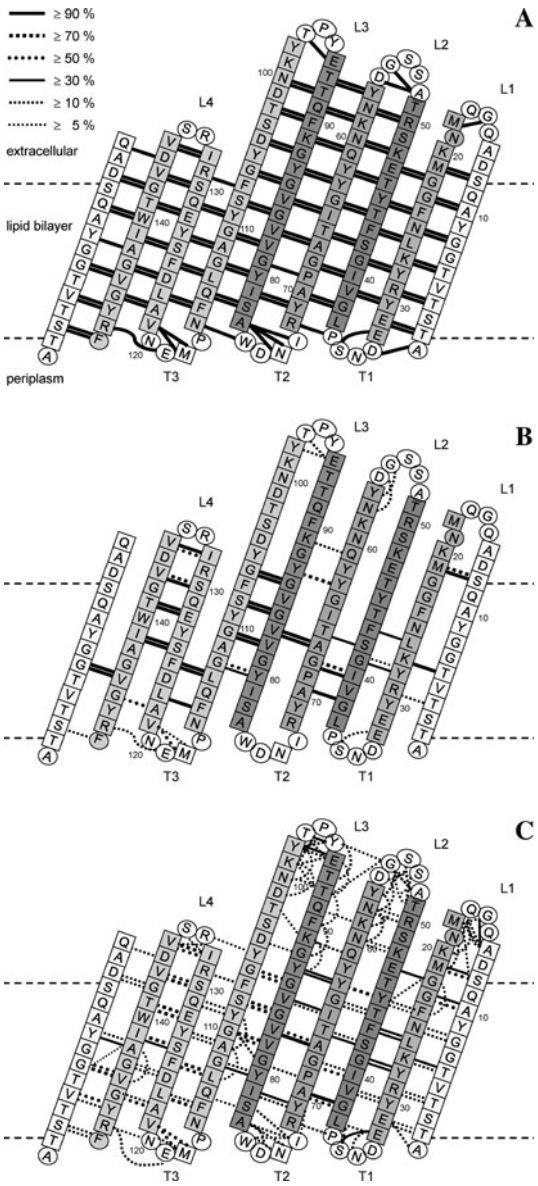

Fig. 8 Analysis of the intra-molecular backbone–backbone hydrogen bonds in the X-ray and NMR structures. The hydrogen bonds are determined by applying the standard GROMOS criterion (see "Methods" section for details) and are represented by a *line*. *Different line thicknesses and types* are used to quantify the population of hydrogen bonds. **a** Hydrogen bonds identified in the X-ray structure, **b** and **c** hydrogen bonds in the set of NMR model structures obtained without and with hydrogen-bond restraining respectively. In the topology plots of the protein, the first strand is shown twice. Residues in β-strands are shown in *squares*, other residues in *circles*, according to the secondary structure assignment of the X-ray structure (Vogt and Schultz 1999). *T* Turn, *L* Loop

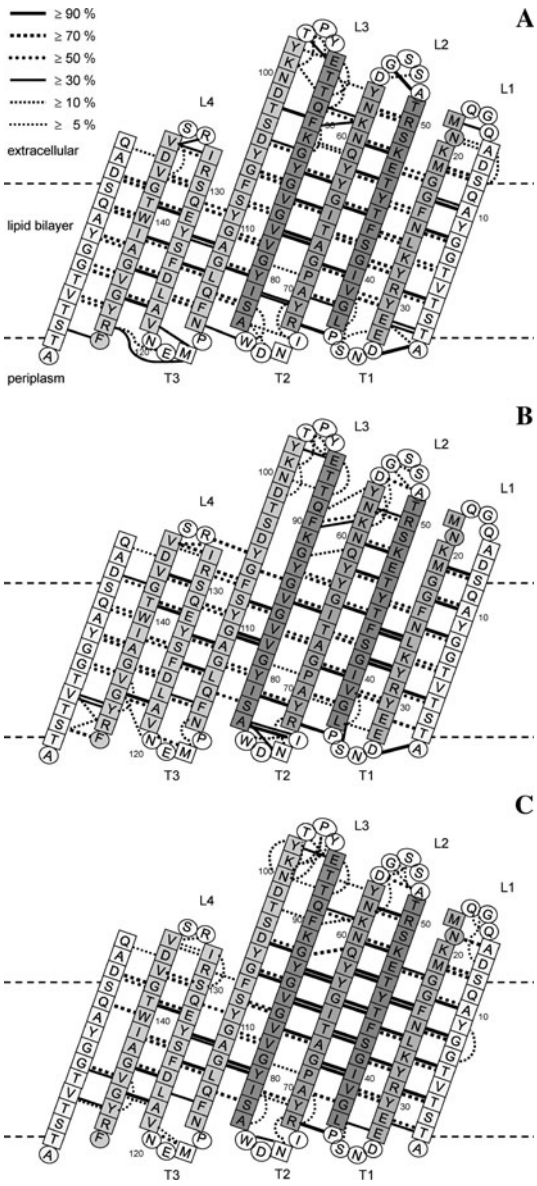

Fig. 9 Analysis of the intra-molecular backbone–backbone hydrogen bonds in the three MD simulations. Simulation OmpX-DMPC-1 (**a**), OmpX-DMPC-2 (**b**) and OmpX-DHPC (**c**). For more details, see Fig. 8

to be at the level of the lipid head groups (which have a broader distribution in the micelle). The protein-water interface is larger in the bilayer than in the micelle. A micellar environment is clearly not identical with a bilayer environment in terms of possible interactions the protein can build with the surrounding lipids, and it is particularly striking that the β-barrel was shortened in the bilayer simulation in order to favour interactions of OmpX residues with the lipids. The protein slightly adapts its structure to fit into the phospholipid environment and favours interactions between amino acid side chains and specific regions of the lipids. This suggests that structures of membrane proteins embedded in a micelle (X-ray, NMR or MD) may be only partially representative of the protein in a physiological membrane environment. Recently NOEs between lipids and OmpX inserted in a bicelle were measured and compared to those obtained from corresponding measurements with OmpX inserted in a micelle, and

Table 7 Hydrogen bond presence between side chains inside the β-barrel over the entire simulation time for OmpX-DMPC-1, OmpX-DMPC-2 and OmpX-DHPC

Hydrogen bond	OmpX-DMPC-1 (%)	OmpX-DMPC-2 (%)	OmpX-DHPC (%)
6Thr–124Asp	61	29	–
12Ser–139Thr	96	81	89
25Asn–42Ser	68	74	–
25Asn–44Thr	47	63	–
27Lys–80Tyr	54	–	72
27Lys–124Asp	75	77	–
29Arg–114Gln	85	7	16
29Arg–78Ser	70	–	14
44Thr–128Glu	67	81	55
46Thr–12Ser	98	62	98
62Tyr–128Glu	99	95	97
66Thr–128Glu	99	42	47
80Tyr–124Asp	99	68	99
108Ser–62Tyr	80	53	79
130Ser–108Ser	48	60	63

The percentages of the different hydrogen bonds between the different atoms of each pair of side chains have been added, yielding the percentage listed. Side chain pairs with hydrogen bonds present more than 60% of the time in one of the simulations were selected and are shown for all three simulations

Table 8 Hydrogen bond presence between side chains and water molecules inside the β-barrel over the entire simulation time for OmpX-DMPC-2 and OmpX-DHPC

Hydrogen bond	OmpX-DMPC-2 (%)	OmpX-DHPC (%)
H_2O–25Asn	31	83
H_2O–42Ser	46	57
H_2O–64Thr	54	19
H_2O–66Thr	24	43
H_2O–124Asp	33	81
H_2O–126Ser	32	9
H_2O–128Glu	70	73
H_2O–130Ser	16	–
H_2O–139Thr	86	19
H_2O–140Trp	–	75

The occurrences of different hydrogen bonds between the indicated side chains and water molecules have been added. Hydrogen bonds present more than 10% of the time in one of the simulations were selected

differences between the two systems were reported (Lee et al. 2008). Structural measurements performed under standard crystallographic environments (detergent milieu) have also been shown to be partially insufficient to observe certain properties of membrane proteins (Long et al. 2007).

Table 9 Hydrogen bond presence between side chains and lipid molecules outside the β-barrel over the entire simulation time for OmpX-DMPC-2 and OmpX-DHPC

Hydrogen bond	OmpX-DMPC-2 (%)	OmpX-DHPC (%)
Lipid–11Gln	–	100
Lipid–17Gln	82	9
Lipid–28Tyr	83	40
Lipid–30Tyr	20	66
Lipid–35Ser	44	82
Lipid–38Gly	–	54
Lipid–48Lys	–	69
Lipid–57Tyr	20	–
Lipid–61Gln	51	–
Lipid–71Tyr	90	99
Lipid–72Arg	11	32
Lipid–73Ile	–	88
Lipid–74Asn	71	98
Lipid–76Trp	–	22
Lipid–77Ala	–	96
Lipid–105Tyr	35	53
Lipid–107Phe	–	23
Lipid–109Tyr	–	99
Lipid–115Phe	–	30
Lipid–116Asn	93	93
Lipid–119Glu	–	39
Lipid–120Asn	19	79
Lipid–127Tyr	79	100
Lipid–129Gln	100	62
Lipid–131Arg	29	–
Lipid–142Ala	–	81
Lipid–146Tyr	11	98
Lipid–147Arg	97	15

The occurrences of different hydrogen bonds between the indicated side chains and the lipids have been added. Hydrogen bonds present more than 20% of the time in one of the simulations were selected

Conclusions

The bacterial outer membrane protein OmpX from *Escherichia coli* has been simulated embedded in a phospholipid bilayer and in a protein-micelle aggregate. A total of three simulations of various lengths between 15 and 25 ns have been performed.

The structural analysis of the three trajectories shows that the protein is stable in all three simulations. In particular, the β-barrel embedded in the lipids shows small atom-positional fluctuations and a stable pattern of interstrand backbone hydrogen bonds, whereas the extracellular part of the protein shows larger structural fluctuations. These results are in satisfactory agreement with experimental observations, in particular with amide proton

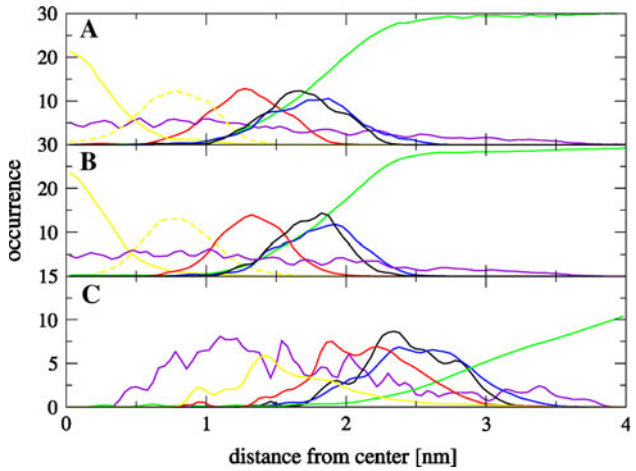

Fig. 10 Distribution of selected atoms in the three MD simulations. OmpX-DMPC-1 (**a**), OmpX-DMPC-2 (**b**) and OmpX-DHPC (**c**). Water in *green*, nitrogen (lipids) in *blue*, phosphate in *black*, oxygen (lipids) in *red*, last carbon in lipid tail in *yellow*, intermediate carbon in tail in *dotted yellow* (not for DHPC), protein N atoms in *violet*. The water curve was divided by 6 for clarity in **a** and **b** and by 3 in **c**. The distribution is given for the distance from the centre of the bilayer or of the micelle respectively. The analysis was performed at 1ps time intervals. See method A for distributions calculations in "Methods" section for details

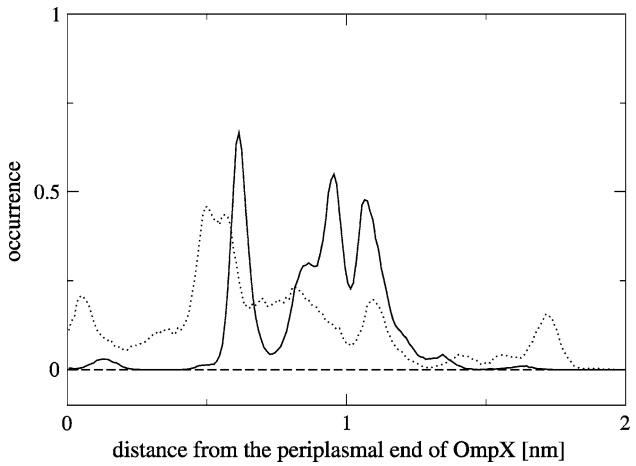

Fig. 11 Water distribution along the axis of the β-barrel in the three MD simulations: OmpX-DMPC-1 in *dashed*, OmpX-DMPC-2 in *dotted*, and OmpX-DHPC in *solid*. See method B for distributions calculations in "Methods" section for details

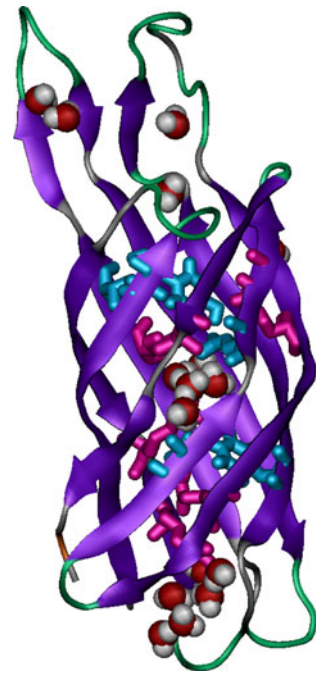

Fig. 12 Water molecules trapped by hydrogen bonds inside the β-barrel for the OmpX-DHPC simulation are shown as *red* and *grey* space-filling models. Residues for which intra-molecular hydrogen bonds are present for more than 90% or between 20 and 90% of the simulation time are drawn as *pink* or *blue* stick diagrams respectively

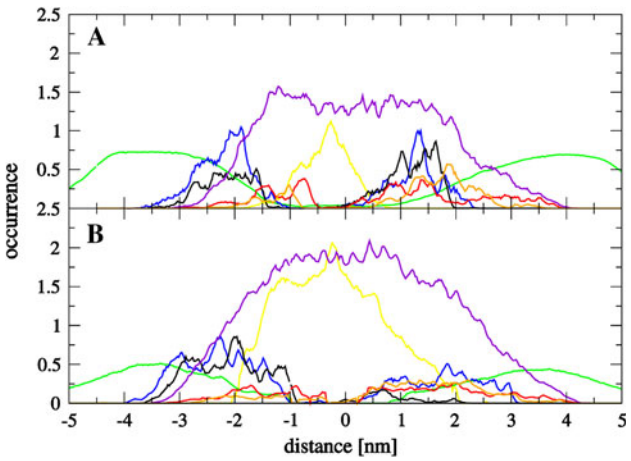

Fig. 13 Distribution of atoms closest to the β-barrel along the axis through the barrel. OmpX-DMPC-2 (**a**) and OmpX-DHPC (**b**). Water is shown in *green*, nitrogen (lipids) in *blue*, phosphate in *black*, last carbon in lipid tail in *yellow*, protein nitrogen atoms in *violet*, lysine and arginine in *orange*, tyrosine and tryptophan in *red*. The protein curves were divided by 4 for clarity. See method C for distributions calculations in "Methods" section for details

exchange experiments (Fernández et al. 2004), and seem to support the postulated role of the protruding β-sheet as a 'waving flag' that is important for interactions with binding partners in the extracellular space (Vogt and Schultz 1999).

The simulations compare well to isotropic atomic B-factors derived from X-ray diffraction data (Vogt and Schultz 1999). Here, we had the opportunity to compare the simulation results not only with crystallographic data, but also with inter-protein NOEs and NOEs between protein and lipid molecules. The simulations compare well also with these experimental data (Fernández et al. 2002, 2004).

All three simulations show a hydrogen-bonding network typical for anti-parallel β-strands. As for the interior of the protein, the protein-protein and water-protein hydrogen bonds do not allow a continuous water flux. In the simulation that started without water inside the barrel of OmpX, no water was observed to enter the interior of the protein, while in the other two simulations occasional exchange of water molecules with bulk water could be observed.

Lysine, tryptophan, arginine and tyrosine residues form numerous hydrogen bonds with the lipid head groups and probably help to position the protein in an energetically favourable manner inside the micelle or the bilayer. Charged amino acids with long side chains as well as aromatic amino acids have been proposed to play a crucial role in membrane protein positioning (Deol et al. 2004; Heijne 1994; Schiffer et al. 1992; Schulz 1993; Strandberg and Killian 2003; Ulmschneider et al. 2001). Actually, because the micelle is slightly wider than the bilayer, the initial structure of OmpX (which originates from a micellar system) seems to compress itself during the course of the MD simulation and the β-barrel shortens to adapt to the width of the bilayer. Experimental NOEs seem to confirm a difference in interactions between lipids and membrane proteins embedded in micelles compared to bicelles (Lee et al. 2008). In view of these considerations, it would be interesting to supplement experimental data on membrane proteins in micellar and bilayer environments with simulations starting from NMR structures obtained in micellar and bicellar environments. Unfortunately the experimental data necessary to perform such studies are not yet available. However, progress is being made towards collecting NMR data from membrane proteins in bilayers (solid-state NMR) (Mahalakshmi and Marassi 2008) and bicelles (liquid NMR) (Lee et al. 2008) and towards collecting crystallographic data in environments more closely related to physiological conditions (Long et al. 2007), which will hopefully soon lead to new experimental structures. Computational studies can then be expected to contribute new insights into the extent to which data from membrane proteins in micelle or other detergent milieu can relate to the situation in the physiological membrane environment. Together with the availability of more experimental data on the differential activity of membrane proteins in different lipid environments (Sanders and Landis 1995), this might further enable an assessment of the importance of lipid-milieu-induced structural and dynamical differences for the physiological function of OmpX and other membrane proteins, which is currently a matter of debate (Matthews et al. 2006).

Acknowledgments Financial support was obtained from the ETH Zürich and the Swiss National Science Foundation through the National Center of Competence in Research (NCCR) Structural Biology (K.W., W.F.G.) and grant no. 200020-121913 (W.F.G.), which is gratefully acknowledged.

References

Arora A, Abildgaard F, Bushweller JH, Tamm LK (2001) Structure of outer membrane protein A transmembrane domain by NMR spectroscopy. Nat Struct Biol 8(4):334–338. doi:10.1038/86214

Berendsen HJC, Postma JPM, van Gunsteren WF, Hermans J (1981) Interaction models for water in relation to protein hydration. In: Pullman B (ed) Intermolecular forces. Reidel, Dordrecht, pp 331–342

Berendsen HJC, Postma JPM, van Gunsteren WF, DiNola A, Haak JR (1984) Molecular dynamics with coupling to an external bath. J Chem Phys 81(8):3684–3690. doi:10.1063/1.448118

Billeter M, Wagner G, Wüthrich K (2008) Solution NMR structure determination of proteins revisited. J Biomol NMR 42(3):155–158. doi:10.1007/s10858-008-9277-8

Böckmann RA, Caflisch A (2005) Spontaneous formation of detergent micelles around the outer membrane protein OmpX. Biophys J 88(5):3191–3204. doi:10.1529/biophysj.105.060426

Bond PJ, Sansom MSP (2003) Membrane protein dynamics versus environment: simulations of OmpA in a micelle and in a bilayer. J Mol Biol 329(5):1035–1053. doi:10.1016/S0022-2836(0310.1016/S0022-2836(03)00408-X

Bond PJ, Faraldo-Gómez JD, Deol SS, Sansom MSP (2006) Membrane protein dynamics and detergent interactions within a crystal: a simulation study of OmpA. Proc Natl Acad Sci USA 103(25):9518–9523. doi:10.1073/pnas.0600398103

Chandrasekhar I, Kastenholz M, Lins RD, Oostenbrink C, Schuler LD, Tieleman DP, van Gunsteren WF (2003) A consistent potential energy parameter set for lipids: dipalmitoylphosphatidylcholine as a benchmark of the GROMOS96 45A3 force field. Eur Biophys J 32(1):67–77. doi:10.1007/s00249-002-0269-4

Cherezov V, Rosenbaum DM, Hanson MA, Rasmussen SGF, Thian FS, Kobilka TS, Choi HJ, Kuhn P, Weis WI, Kobilka BK, Stevens RC (2007) High-resolution crystal structure of an engineered human 2-adrenergic G protein coupled receptor. Science 318(5854):1258–1265. doi:10.1126/science.1150577

Chiu S, Clark M, Balaji V, Subramaniam S, Scott H, Jakobsson E (1995) Incorporation of surface tension into molecular dynamics simulation of an interface: a fluid phase lipid bilayer membrane. Biophys J 69(4):1230–1245. doi:10.1016/S0006-3495(95)80005-6

Chou JJ, Kaufman JD, Stahl SJ, Wingfield PT, Bax A (2002) Micelle-induced curvature in a water-insoluble HIV-1 Env peptide revealed by NMR dipolar coupling measurement in stretched polyacrylamide gel. J Am Chem Soc 124(11):2450–2451. doi:10.1021/ja017875d

Colombo G, Marrink SJ, Mark AE (2003) Simulation of MscL gating in a bilayer under stress. Biophys J 84(4):2331–2337. doi:10.1016/S0006-3495(03)75038-3

de Planque MRR, Bonev BB, Demmers JA, Greathouse DV, Koeppe RE, Separovic F, Watts A, Killian AJ (2003) Interfacial anchor properties of tryptophan residues in transmembrane peptides can dominate over hydrophobic matching effects in peptide-lipid interactions. Biochemistry 42(18):5341–5348. doi:10.1021/bi027000r

Deol SS, Bond PJ, Domene C, Sansom MSP (2004) Lipid-protein interactions of integral membrane proteins: a comparative simulation study. Biophys J 87(6):3737–3749. doi:10.1529/biophysj.104.048397

Domene C, Sansom MSP, Bond PJ (2003) Membrane protein simulations: ion channels and bacterial outer membrane proteins.

Adv Protein Chem 66:159–193. doi:10.1016/S0065-3233(03)66005-5

Fernández C, Wider G (2003) TROSY in NMR studies of the structure and function of large biological macromolecules. Curr Opin Struct Biol 13(5):570–580. doi:10.1016/j.sbi.2003.09.009

Fernández C, Wüthrich K (2003) NMR solution structure determination of membrane proteins reconstituted in detergent micelles. FEBS Lett 555(1):144–150. doi:10.1016/S0014-5793(03)01155-4

Fernández C, Adeishvili K, Wüthrich K (2001a) Transverse relaxation-optimized NMR spectroscopy with the outer membrane protein OmpX in dihexanoyl phosphatidylcholine micelles. Proc Natl Acad Sci USA 98(5):2358–2363. doi:10.1073/pnas.051629298

Fernández C, Hilty C, Bonjour S, Adeishvili K, Pervushin K, Wüthrich K (2001b) Solution NMR studies of the integral membrane proteins OmpX and OmpA from *Escherichia coli*. FEBS Lett 504(3):173–178. doi:10.1016/S0014-5793(01)02742-9

Fernández C, Hilty C, Wider G, Wüthrich K (2002) Lipid-protein interactions in DHPC micelles containing the integral membrane protein OmpX investigated by NMR spectroscopy. Proc Natl Acad Sci USA 99(21):13533–13537. doi:10.1073/pnas.212515099

Fernández C, Hilty C, Wider G, Güntert P, Wüthrich K (2004) NMR structure of the integral membrane protein OmpX. J Mol Biol 336(5):1211–1221. doi:10.1016/j.jmb.2003.09.014

Frishman DD, Argos P (1995) Knowledge-based protein secondary structure assignment. Proteins 23(4):566–579. doi:10.1002/prot.340230412

Gerber S, Comellas-Bigler M, Goetz BA, Locher KP (2008) Structural basis of trans-inhibition in a molybdate/tungstate ABC transporter. Science 321(5886):246–250. doi:10.1126/science.1156213

Hanson MA, Cherezov V, Griffith MT, Roth CB, Jaakola VP, Chien EYT, Velasquez J, Kuhn P, Stevens RC (2008) A specific cholesterol binding site is established by the 2.8 Å structure of the human β2-adrenergic receptor. Structure 16(6):897–905. doi:10.1016/j.str.2008.05.001

Heijne GV (1994) Membrane proteins: from sequence to structure. Annu Rev Biophys Biomol Struct 23(1):167–192. doi:10.1146/annurev.bb.23.060194.001123

Hilf RJC, Dutzler R (2008) Structure of a potentially open state of a proton-activated pentameric ligand-gated ion channel. Nature 457(7225):115–118. doi:10.1038/nature07461

Hiller S, Garces RG, Malia TJ, Orekhov VY, Colombini M, Wagner G (2008) Solution structure of the integral human membrane protein VDAC-1 in detergent micelles. Science 321(5893):1206–1210. doi:10.1126/science.1161302

Hilty C, Fernández C, Wider G, Wüthrich K (2002) Side chain NMR assignments in the membrane protein OmpX reconstituted in DHPC micelles. J Biomol NMR 23(4):289–301. doi:10.1023/A:1020218419190

Hilty C, Wider G, Fernández C, Wüthrich K (2003) Stereospecific assignments of the isopropyl methyl groups of the membrane protein OmpX in DHPC micelles. J Biomol NMR 27(4):377–382. doi:10.1023/A:1025877326533

Hilty C, Wider G, Fernández C, Wüthrich K (2004) Membrane protein-lipid interactions in mixed micelles studied by NMR spectroscopy with the use of paramagnetic reagents. ChemBioChem 5(4):467–473. doi:10.1002/cbic.200300815

Hub JS, de Groot BL (2008) Mechanism of selectivity in aquaporins and aquaglyceroporins. Proc Natl Acad Sci USA 105(4):1198–1203. doi:10.1073/pnas.0707662104

Hub JS, Grubmüller H, de Groot BL (2005) The dynamics and energetics of water permeation and proton exclusion in aquaporins. Curr Opin Struct Biol 15(2):176–183. doi:10.1016/j.sbi.2005.02.00

Hünenberger PH, Mark AE, van Gunsteren WF (1995) Fluctuation and cross-correlation analysis of protein motions observed in nanosecond molecular dynamics simulations. J Mol Biol 252(4):492–503. doi:10.1006/jmbi.1995.0514

Kabsch W, Sander C (1983) Dictionary of protein secondary structure: pattern recognition of hydrogen-bonded and geometrical features. Biopolymers 22(12):2577–2637. doi:10.1002/bip.360221211

Kadaba NS, Kaiser JT, Johnson E, Lee A, Rees DC (2008) The high-affinity *E. coli* methionine ABC transporter: structure and allosteric regulation. Science 321(5886):250–253. doi:10.1126/science.1157987

Khalid S, Bond P, Carpenter T, Sansom M (2008) Ompa: gating and dynamics via molecular dynamics simulations. Biochim Biophys Acta Biomemb 1778(9):1871–1880. doi:10.1016/j.bbamem.2007.05.024

Kleinschmidt JH, Tamm LK (1996) Folding intermediates of a β-barrel membrane protein. Kinetic evidence for a multi-step membrane insertion mechanism. Biochemistry 35(40):12993–13266. doi:10.1021/bi961478b

Landolt-Marticorena C, Williams KA, Deber CM, Reithmeier RAF (1993) Non-random distribution of amino acids in the transmembrane segments of human type I single span membrane proteins. J Mol Biol 229(3):602–608. doi:10.1006/jmbi.1993.1066

Lee D, Walter KFA, Brückner A, Hilty C, Becker S, Griesinger C (2008) Bilayer in small bicelles revealed by lipid protein interactions using NMR spectroscopy. J Am Chem Soc 130(42):13822–13823. doi:10.1021/ja803686p

Lin X, Wu L, Li H, Wang S, Peng X (2008) Downregulation of Tsx and OmpW and upregulation of OmpX are required for iron homeostasis in *Escherichia coli*. J Proteome Res 7(3):1235–1243. doi:10.1021/pr7005928

Long SB, Tao X, Campbell EB, MacKinnon R (2007) Atomic structure of a voltage-dependent K+ channel in a lipid membrane-like environment. Nature 450(7168):376–382. doi:10.1038/nature06265

MacCallum JL, Bennett WFD, Tieleman DP (2008) Distribution of amino acids in a lipid bilayer from computer simulations. Biophys J 94(9):3393–3404. doi:10.1529/biophysj.107.112805

Mahalakshmi R, Marassi FM (2008) Orientation of the *Escherichia coli* outer membrane protein OmpX in phospholipid bilayer membranes determined by solid-state NMR. Biochemistry 47(25):6531–6538. doi:10.1021/bi800362b

Marassi F, Opella SJ (1998) NMR structural studies of membrane proteins. Curr Opin Struct Biol 8(5):640–648. doi:10.1016/S0959-440X(98)80157-7

Matthews EE, Zoonens M, Engelman DM (2006) Dynamic helix interactions in transmembrane signaling. Cell 127(3):447–450. doi:10.1016/j.cell.2006.10.016

Nagle JF, Tristram-Nagle S (2000) Structure of lipid bilayers. Biochim Biophys Acta 1469(3):159–195. doi:10.1016/S0304-4157(00)00016-2

Ostermeier C, Michel H (1997) Crystallization of membrane proteins. Curr Opin Struct Biol 7(5):697–701. doi:10.1016/S0959-440X(97)80080-2

Pautsch A, Schulz GE (2000) High-resolution structure of the OmpA membrane domain. J Mol Biol 298(2):273–282. doi:10.1006/jmbi.2000.367

Pervushin K, Riek R, Wider G, Wüthrich K (1997) Attenuated T2 relaxation by mutual cancellation of dipole-dipole coupling and chemical shift anisotropy indicates an avenue to NMR structures of very large biological macromolecules in solution. Proc Natl Acad Sci USA 94(23):12366–12371. doi:10.1073/pnas.94.23.12366

Ryckaert JP, Ciccotti G, Berendsen HJC (1977) Numerical integration of the cartesian equations of motion of a system with constraints: molecular dynamics of n-alkanes. J Comp Phys 23(3):327–341. doi:10.1016/0021-9991(77)90098-5

Sanders CR, Landis GC (1995) Reconstitution of membrane proteins into lipid-rich bilayered mixed micelles for NMR studies. Biochemistry 34(12):4030–4040. doi:10.1021/bi00012a022

Schiffer M, Chang CH, Stevens FJ (1992) The functions of tryptophan residues in membrane proteins. Protein Eng 5(3):213–214. doi:10.1093/protein/5.3.213

Schuler LD, Xaura D, van Gunsteren WF (2001) An improved GROMOS96 force field for aliphatic hydrocarbons in the condensed phase. J Comput Chem 22(11):1205–1218. doi:10.1002/jcc.1078

Schulz GE (1993) Bacterial porins: structure and function. Curr Opin Cell Biol 5(4):701–707. doi:10.1016/0955-0674(93)90143-E

Schulz GE (2002) The structure of bacterial outer membrane proteins. Biochim Biophys Acta Biomemb 1565(2):2450–2451. doi:10.1016/S0005-2736(02)00577-1

Scott WRP, Hünenberger PH, Tironi IG, Mark AE, Billeter SR, Fennen J, Torda AE, Huber T, Krüger P, van Gunsteren WF (1999) The GROMOS biomolecular simulation program package. J Phys Chem A 103(19):3596–3607. doi:10.1021/jp984217f

Shrivastava IH, Tieleman DP, Biggin PC, Sansom MSP (2002) K+ versus Na+ ions in a K channel selectivity filter: a simulation study. Biophys J 83(2):633–645. doi:10.1016/S0006-3495(02)75197-7

Smith P, van Gunsteren WF (1994) Consistent dielectric properties of the simple point charge and extended simple point charge water models at 277 and 300 K. J Chem Phys 100(4):3169–3174. doi:10.1063/1.466407

Soares TA, Daura X, Oostenbrink C, Smith LJ, van Gunsteren WF (2004) Validation of the GROMOS force-field parameter set 45A3 against nuclear magnetic resonance data of hen egg lysozyme. J Biomol NMR 30(4):407–422. doi:10.1007/s10858-004-5430-1

Stocker U, Spiegel K, van Gunsteren WF (2000) On the similarity of properties in solution or in the crystalline state: a molecular dynamics study of hen lysozyme. J Biomol NMR 18(1):1–12. doi:10.1023/A:1008379605403

Strandberg E, Killian JA (2003) Snorkeling of lysine side chains in transmembrane helices: how easy can it get? FEBS Lett 544(1):69–73. doi:10.1016/S0014-5793(03)00475-7

Sun H, Greathouse DV, Andersen OF, Koeppe RE (2008) On the preference of tryptophan for membrane interfaces: insights from n-methylation of tryptophans in gramicidin channels. J Biol Chem 283:22233–22243. doi:10.1074/jbc.M802074200

Ulmschneider MB, Tieleman DP, Sansom MSP (2001) Amino acid distributions in integral membrane protein structures. Biochim Biophys Acta Biomemb 1512(1):1–14. doi:10.1016/S0005-2736(01)00299-1

Valiyaveetil FI, Zhou Y, MacKinnon R (2002) Lipids in the structure, folding, and function of the KcsA K+ channel. Biochemistry 41(35):10771–10777. doi:10.1021/bi026215y

van Gunsteren WF, Billeter SR, Eising A, Hünenberger PH, Krüger P, Mark A, Scott WRP, Tironi IG (1996) Biomolecular simulation: the GROMOS96 manual und user guide. Hochschulverlag an der ETH Zürich, Zürich

van Gunsteren WF, Bakowies D, Baron R, Chandrasekhar I, Christen M, Daura X, Gee P, Geerke DP, Glättli A, Hünenberger PH, Kastenholz MA, Oostenbrink C, Schenk M, Trzesniak D, van der Vegt NFA, Yu HB (2006) Biomolecular modeling: goals, problems, perspectives. Angew Chem Int Ed 45(25):4064–4092. doi:10.1002/anie.200502655

van Horn WD, Kim HJ, Ellis CD, Hadziselimovic A, Sulistijo ES, Karra MD, Tian C, Sonnichsen FD, Sanders CR (2009) Solution nuclear magnetic resonance structure of membrane-integral diacylglycerol kinase. Science 324(5935):1726–1729. doi:10.1126/science.1171716

Vogt J, Schultz GE (1999) The structure of the outer membrane protein OmpX from *Escherichia coli* reveals possible mechanisms of virulence. Structure 7(10):1301–1309. doi:10.1016/S0969-2126(00)80063-5

Wallin E, von Heijne G (1998) Genome-wide analysis of integral membrane proteins from eubacterial, archaean, and eukaryotic organisms. Protein Sci 7(4):1029–1038. doi:10.1002/pro.5560070420

Wassenaar TA, Daura X, Padros E, Mark AE (2009) Calcium binding to the purple membrane: a molecular dynamics study. Proteins 74(3):669–681. doi:10.1002/prot.22182

Wimley WC (2002) Toward genomic identification of β-barrel membrane proteins: composition and architecture of known structures. Protein Sci 11(2):301–312. doi:10.1110/ps.29402

Wüthrich K, Braun W, Billeter M (1983) Pseudo-structures for the 20 common amino acids for use in studies of protein conformations by measurements of intramolecular proton-proton distance constraints with nuclear magnetic resonance. J Mol Biol 169(4):9490-961. doi:10.1016/S0022-2836(83)80144-2

Yau WM, Wimley WC, Gawrisch K, White SH (1998) The preference of tryptophan for membrane interfaces. Biochemistry 37(42):14713–14718. doi:10.1021/bi980809c